J. Fluid Mech. (1993), *vol.* 250, *pp.* 553–586

Barotropic flow over finite isolated topography: steady solutions on the beta-plane and the initial value problem

By LUANNE THOMPSON[1] AND GLENN R. FLIERL[2]

[1] School of Oceanography WB-10, University of Washington, Seattle, WA 98195, USA

[2] Massachussetts Institute of Technology, 54–1426, Cambridge, MA 02139, USA

(Received 8 November 1991 and in revised form 24 November 1992)

Solutions for inviscid rotating flow over a right circular cylinder of finite height are studied, and comparisons are made to quasi-geostrophic solutions. To study the combined effects of finite topography and the variation of the Coriolis parameter with latitude a steady inviscid model is used. The analytical solution consists of one part which is similar to the quasi-geostrophic solution that is driven by the potential vorticity anomaly over the topography, and another, similar to the solution of potential flow around a cylinder, that is driven by the matching conditions on the edge of the topography. When the characteristic Rossby wave speed is much larger than the background flow velocity, the transport over the topography is enhanced as the streamlines follow lines of constant background potential vorticity. For eastward flow, the Rossby wave drag can be very much larger than that predicted by quasi-geostrophic theory. The combined effects of finite height topography and time-dependence are studied in the inviscid initial value problem on the f-plane using the method of contour dynamics. The method is modified to handle finite topography. When the topography takes up most of the layer depth, a stable oscillation exists with all of the fluid which originates over the topography rotating around the topography. When the Rossby number is order one, a steady trapped vortex solution similar to the one described by Johnson (1978) may be reached.

1. Introduction

Taylor (1917) discovered that a homogeneous and rapidly rotating fluid has flow nearly independent of the coordinate parallel to the axis of rotation. He observed in the laboratory that, because of this effect, flow tended to go around instead of over a topographic feature, leaving an undisturbed column over the topography (Taylor 1923). This phenomenon was dubbed a Taylor column by Hide (1961). Most modelling efforts have concentrated on studying flow which has a time-scale small compared to the rotation period, and topography which takes up a small fraction of the total layer depth so that the quasi-geostrophic approximation can be employed. This approximation is amenable to the use of analytical methods. Under the quasi-geostrophic approximation, the effects of nonlinearities without the influence of friction have been studied extensively, including both the β-effect and stratification (Hupport 1975; Janowitz 1975; McCartney 1975; Johnson 1977, 1979). In these solutions, the flow is found by assuming that the potential vorticity–stream function relationship $q(\psi)$ is determined from upstream conditions. However, once streamlines close, this relationship is no longer uniquely determined because some fluid within closed

streamlines does not necessarily originate upstream. There have been several attempts to close the problem sensibly. The approach followed in the studies mentioned above was to allow the upstream $q(\psi)$ to hold within closed streamlines.

Another consistent inviscid solution allows the fluid to be stagnant within closed streamlines (ψ = constant). Ingersoll (1969) showed that this solution is the same as including the effect of bottom drag in the limit of vanishing viscosity. Johnson (1983) showed that this same solution is also consistent with requiring that the maximum amount of fluid be retained over the topography in the initial value problem (he termed these solutions maximum retention solutions). Johnson (1978) found an additional steady solution by using a variational principle to describe steady motions at finite Rossby number over obstacles of finite height. In this solution, the fluid which originated over the topography in the initial value problem is moved off as a trapped vortex located to the right (looking downstream) of the topography.

This problem has also been considered in the laboratory. McCartney (1975) simulated in the laboratory barotropic flow over topography in the β-plane. He demonstrated that lee Rossby waves are generated downstream of the topography as predicted by his theory. Boyer, Davies & Holland (1984) revisted this problem in the laboratory and numerically. They again observed the generation of damped lee Rossby waves. Friction is important in the laboratory and was also included in their numerical solutions of the steady problem.

Steady solutions give useful insight into important dynamical processes. However, it is unclear under what circumstances the various steady solutions described above would be obtained, and there are an infinite number of additional steady solutions to the inviscid problem when closed streamlines occur. Huppert & Bryan (1976) solved the initial value problem for flow over topography in a periodic domain using a primitive equation model with continuous stratification on the f-plane. Although the integration time was short so the steady state was not reached, they suggested that two different flow regimes are possible, one in which the fluid which originated over the topography was trapped there, and one in which it escaped downstream. James (1980) realized that much of the dynamics that Huppert & Bryan (1976) found could be explained in a much simpler barotropic quasi-geostrophic context. He found that when some fluid was trapped over the topography, a patch of positive vorticity spirals onto the hill, while successive pieces of it broke away and then coalesced back into the main patch of positive vorticity. Bannon (1980) solved the initial value problem for flow on the β-plane over finite Gaussian topography to find the steady solution, but included frictional effects and found solutions for only a limited range of the parameters. Verron & Le Provost (1985) studied the problem on the β-plane, where Rossby waves were generated downstream of the topography for eastward flow. These solutions were limited because the model was confined to a channel in y (the north–south direction), and not run to steady state. All of these modelling studies were done using finite difference algorithms and thus included frictional effects. Kozlov (1983) studied the inviscid quasi-geostrophic problem for cylindrical topography using the method of contour dynamics and found similar behaviour to that described above.

In order to extend the above work, we consider flow over finite topography in a simplified geometry, barotropic flow with a rigid lid over a right circular cylinder. Throughout, we discuss the validity of the quasi-geostrophic solution. In §2, we explore combining the β-effect with finite topography. Because of the simple geometry a systematic exploration of the parameter space of the obstacle height, the strength of the flow, and the horizontal scale of the topography can be made using the analytic solution. The drag, the lift, and the transport over the topography are discussed. In §3,

the initial value problem is discussed for flow on the f-plane using contour dynamics. A modified contour dynamics method is developed and the relationship to steady-state solutions is discussed.

2. Steady solutions on the β-plane

2.1. *Model formulation*

For inviscid flow in shallow water with a rigid lid on the β-plane, the momentum equation is

$$\mathrm{d}\boldsymbol{u}/\mathrm{d}t+(f_0+\beta y)(\hat{\boldsymbol{z}}\times\boldsymbol{u})=\boldsymbol{\nabla}P,$$

and the continuity equation is

$$\boldsymbol{\nabla}\cdot h\boldsymbol{u}=0, \tag{1}$$

where

$$\mathrm{d}/\mathrm{d}t=\partial/\partial t+\boldsymbol{u}\cdot\boldsymbol{\nabla}.$$

Here, $\boldsymbol{u}$ is the horizontal velocity, h is the depth of the fluid, P is the pressure, f_0 is the Coriolis parameter, and β the latitudinal derivative of the Coriolis parameter. The coordinate system is z positive upward from the bottom, x is east, y is north and $\boldsymbol{\nabla}$ is the horizontal gradient operator (∂_x, ∂_y). As long as we are considering solutions which exist for times short compared to the frictional timescale (for instance the spindown time), the fluid will be considered to be completely inviscid. The shallow water model is valid as long as the vertical variations of the horizontal velocity can be ignored. This is true as long as the aspect ratio of the fluid is small (that is the ratio of the layer depth to the horizontal lengthscale is small). Bannon (1980) gives a thorough discussion of the validity of the shallow water model in this context. For the beta-plane approximation to be valid, $\beta L/f_0$ where L is the horizontal lengthscale, should be at most order one.

Potential vorticity is conserved following fluid parcels:

$$\mathrm{d}q/\mathrm{d}t=0, \tag{2}$$

where

$$q=(v_x-u_y+f_0+\beta y)/h. \tag{3}$$

A transport stream function can be defined by

$$hu=-\psi_y,$$

and

$$hv=\psi_x$$

where u and v are the zonal and meridional components of the velocity.

In steady state the Bernoulli function, B, is conserved on streamlines, where

$$B=\tfrac{1}{2}u^2+\tfrac{1}{2}v^2+P. \tag{4}$$

Both B and q can be written as functions of ψ in steady state. The functional relationships can be found from the upstream conditions. Assuming that there is a uniform zonal flow of size U upstream of the obstacle,

$$\psi=-UyH,$$

where H is the constant depth of the fluid far away from the bump. Therefore,

$$q(\psi)=\frac{f_0}{H}-\frac{\beta\psi}{UH^2} \tag{5}$$

describes the potential vorticity as long as the fluid parcels have originated upstream.

If ψ is scaled by $|U|HL$ where L is the characteristic radius of the bump, and x and y are scaled by L, then using (3) and (5) the non-dimensional ψ is governed by

$$\nabla\cdot\frac{\nabla\psi}{h}+\frac{b}{V}h\psi=-\frac{1-h}{\epsilon}-by. \tag{6}$$

There are three non-dimensional parameters in the equation: h, the non-dimensional height of the topography scaled by the total depth of the fluid; b, (defined by $\beta L^2/|U|$) the ratio of the Rossby wave speed to the background flow velocity; and the Rossby number $\epsilon=|U|/f_0 L$. In these equations V is either 1 or -1 depending on the direction of the flow.

If h is radially symmetric, then the solution for ψ can be divided into an odd part in $y(\psi_o)$ and an even part in $y(\psi_e)$. The even part is proportional to $1/\epsilon$ and is forced by the first term on the right-hand side of (6), while the odd part is independent of ϵ and forced by the second term on the right-hand side of (6). For westward and f-plane flow ψ is even in x. For an isolated obstacle, the background flow remains undisturbed,

$$\psi\to -Vy$$

for westward and f-plane flow. However, because of the existence of Rossby waves, the far-field boundary conditions introduce upstream–downstream asymmetry for eastward flow:

$$r^{\frac{1}{2}}(\psi+y)\to 0,\quad \tfrac{1}{2}\pi<\theta<\tfrac{3}{2}\pi. \tag{7}$$

This boundary condition comes from allowing no upstream energy propagation by Rossby waves.

In the quasi-geostrophic model, the (q,ψ)-relationship is given by (5), but (6) becomes

$$\nabla^2\psi+\frac{b}{V}\psi=-\frac{1-h}{\epsilon}-by.$$

This simpler problem was solved by McCartney (1975) for flow over a right circular cylinder. The matching conditions are that ψ and ψ_r are continuous across the boundary of the topography. The solution can be written as

$$\psi=-Vy+\phi,$$

where ϕ is independent of U. The only antisymmetric part is $-Vy$. The pressure is equal to ψ which is continuous at $r=1$. The solution has no horizontal divergence.

For simplicity, we consider flow over a right circular cylinder. The topography is given by

$$h=\begin{cases}h_0, & r<1\\ 0, & r>1.\end{cases}$$

To solve for the stream function, two matching conditions are needed at $r=1$. First, by integrating the continuity equation (1) across $r=1$, it can be seen that the mass transport, ψ, must be continuous. Second, we require the tangential velocity, ψ_r/h, to be continuous as in Johnson (1978). This allows the vorticity to be finite at $r=1$. It should be noted that this condition requires that the pressure be discontinuous at $r=1$. This is consistent with the conservation of B and the speeding up of the flow above the topography. In the Appendix we consider the solution for flow over linearly changing topography and show that in the limit of a finite step, the matching conditions reduce to those that we choose here.

The functional relationship between B and ψ can be found from the upstream boundary condition, which gives

$$B(\psi) = \psi - \tfrac{1}{2}V\epsilon b\psi^2. \tag{8}$$

The first term is the geostrophic pressure, the only contribution in quasi-geostrophy. The second term results from the inclusion of β in the finite-depth model and, being proportional to ϵ, vanishes in the quasi-geostrophic limit. Using (4) and (8), the pressure is then

$$P = \psi - \tfrac{1}{2}\psi^2 V\epsilon\beta - \frac{\epsilon}{2h^2}(\psi_r^2 + \psi_\theta^2). \tag{9}$$

To analyse the solutions to (6), several quantities of physical interest are calculated, and the results for these calculations are compared to the results found using the quasi-geostrophic approximation. The magnitude of the circulation Γ induced over the topography is given by

$$\Gamma = \frac{1}{h}\oint \psi_r(1,\theta)\,\mathrm{d}\theta.$$

Since only the symmetric part of the solution contributes to this integral, Γ is proportional to $1/\epsilon$ as Bannon (1980) pointed out. This result is the same for quasi-geostrophic flow. The amount of fluid that goes over the topography relative to the undisturbed flow upstream of the topography is the blocking efficiency.

$$T(y) = 1 - \frac{\psi(y) - \psi(-y)}{2Vy}$$

defined by Bannon (1980). Here, $2Vy$ is the transport approaching the obstacle between y and $-y$ at $x = 0$, and $\psi(y) - \psi(-y)$ is the transport between y and $-y$. Thus, $1 - T$ is the fraction of transport passing over the bump, and T is the fraciton of transport diverted around the bump. When $T > 0$ the flow is blocked, and when $T < 0$ the transport is enhanced. For quasi-geostrophic theory, which does not allow horizontal divergence, none of the fluid is diverted around the obstacle, and $T = 0$. Note that $T(\infty) = 0$, and T depends only on ψ_o, the odd portion of the stream function, and is therefore independent of ϵ as Bannon (1980) and Johnson (1978) pointed out for f-plane flows over radially symmetric topography. The calculation of T does not take into account closed streamlines, which would alter our notion of blocking efficiency. In our calculations, we ignore this effect by evaluating T at $y = 1$, the edge of the topography.

The flow exerts a force on the topography, or conversely, the topography exerts a force on the flow. The force can be divided into the drag, D, the force in the zonal direction, and the lift L, the force in the meridional direction. The forces on the bump are given by

$$\boldsymbol{F} = \int P\nabla h\,\mathrm{d}A.$$

Here, h is discontinuous, $h_r = h_0\,\delta(1-r)$, and the pressure is discontinuous. To evaluate this integral, we let the topography be an approximation to smooth topography, with h_r symmetric about $r = 1$, close to a delta function. As the topography becomes steeper, the integral of Ph_r over r tends toward $h_0\,\frac{1}{2}[P(r = 1^+) + P(r = 1^-)]$. Thus,

$$D = \oint h_0\,\tfrac{1}{2}[P(r = 1^+) + P(r = 1^-)]\cos\theta\,\mathrm{d}\theta$$

and $$L = \oint h_0 \tfrac{1}{2}[P(r=1^+)+P(r=1^-)]\sin\theta\,\mathrm{d}\theta.$$

The pressure can be divided into its odd and even parts $P = P_e + P_o$, where

$$P_o = \psi_o - V\epsilon\beta\psi_e\psi_o - (\epsilon/h^2)(\psi_{e_r}\psi_{o_r}+\psi_{e_\theta}\psi_{o_\theta}),$$

and $$P_e = \psi_e - V\epsilon\beta\tfrac{1}{2}(\psi_e^2+\psi_o^2) - (\epsilon/2h^2)(\psi_{e_r}^2+\psi_{or}^2+\psi_{e_\theta}^2+\psi_{o_\theta}^2).$$

The odd component, P_o, is independent of ϵ so that the lift is independent of ϵ. The even component, P_e, has terms proportional to ϵ and $1/\epsilon$. For westward flow and flow on the f-plane, the pressure is even about the y-axis, so that the drag is zero.

2.2. *Solutions for westward flow on the β-plane*

For westward flow, the introduction of β traps the disturbance near the topography. The quasi-geostrophic approximation gives the solution (McCartney 1975)

$$\psi = r\sin\theta + \frac{h_0}{\epsilon b^{\frac{1}{2}}}\begin{cases} I_1(b^{\frac{1}{2}})\,K_0(b^{\frac{1}{2}}r), & r>1 \\ -K_1(b^{\frac{1}{2}})\,I_0(b^{\frac{1}{2}}r)+1/b^{\frac{1}{2}}, & r<1. \end{cases}$$

The finite-depth solution is

$$\psi = r\sin\theta + a_1 K_0(b^{\frac{1}{2}}r) + a_2 K_1(b^{\frac{1}{2}}r)\sin\theta \quad \text{for} \quad r>1$$

and $$\psi = \frac{r\sin\theta}{1-h_0} + b_1 I_0(\kappa r) + b_2 I_1(\kappa r)\sin\theta + F_0 \quad \text{for} \quad r<1,$$

where $$F_0 = h_0/[\epsilon b(1-h_0)]$$

and $$\kappa^2 = b(1-h_0)^2.$$

The coefficients a_1, a_2, b_1, and b_2 are found using the matching conditions at $r=1$.

When b is large the combined effects of finite topography and β are most striking (figure 1). In this limit, streamlines tend to follow lines of constant background potential vorticity, so that the relative vorticity in the potential vorticity equation can be neglected except in boundary layers at $r=1$. The quasi-geostrophic solution is approximately

$$\psi = r\sin\theta + \frac{h_0}{2\epsilon b}\begin{cases} \mathrm{e}^{-\xi}, & r>1 \\ \mathrm{e}^{\xi}-2, & r<1. \end{cases}$$

where $\chi = (r-1)b^{\frac{1}{2}}$ is the boundary-layer variable. The finite-depth solution is

$$\psi = r\sin\theta + \frac{h_0}{2(1-h_0)}\mathrm{e}^{-\xi}\sin\theta + \frac{h_0}{2(1-h_0)\,\epsilon b}\mathrm{e}^{-\xi} \quad \text{for} \quad r>1$$

and

$$\psi = \frac{r\sin\theta}{1-h_0} - \frac{h_0}{2(1-h_0)}\mathrm{e}^{\xi(1-h_0)}\sin\theta - \frac{h_0}{2(1-h_0)\,\epsilon b}\mathrm{e}^{\xi(1-h_0)} + \frac{h_0}{(1-h_0)\,\epsilon b} \quad \text{for} \quad r<1.$$

Both boundary-layer solutions are correct to order $b^{-\frac{1}{2}}$, while $b\epsilon$ is order 1 and $b \gg 1$. The differences between the quasi-geostrophic solutions and the finite-depth solutions

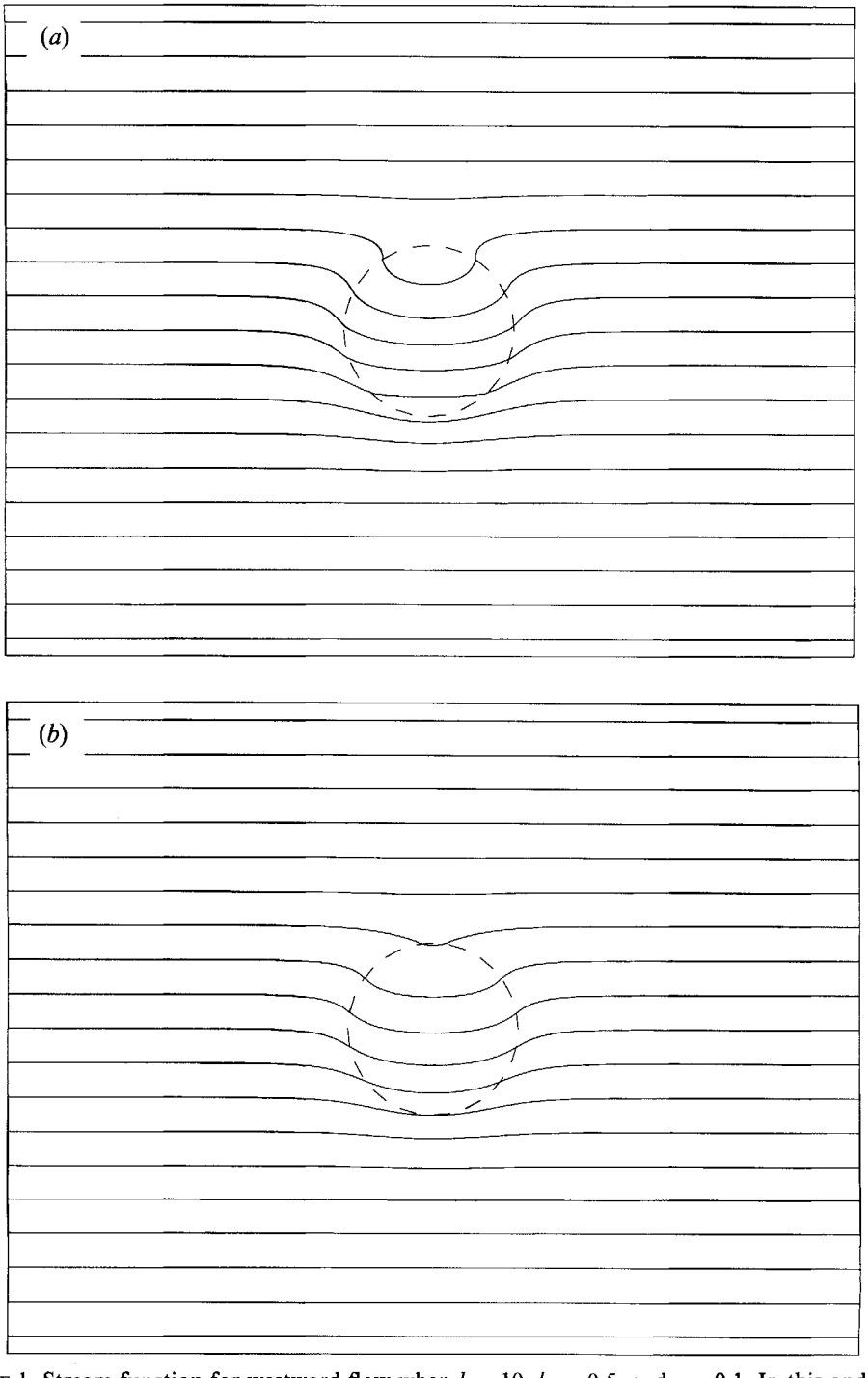

FIGURE 1. Stream function for westward flow when $b = 10$, $h_0 = 0.5$, and $\epsilon = 0.1$. In this and in all subsequent contour plots, the contour interval is 0.4, and the topography is represented by the circle (dashed) with radius 1. (*a*) Finite-depth solution, and (*b*) quasi-geostrophic solution.

can be seen by considering a fluid parcel which originates upstream at $y = y_e$ and has potential vorticity $f_0 + \beta y$. If we move this parcel over the topography to y_i conserving of potential vorticity (neglecting relative vorticity) we have

$$\frac{f_0+\beta y_e}{H} = \frac{f_0+\beta y_i}{H(1-h_0)}$$

so that

$$y_i = y_e(1-h_0) - f_0 h_0/\beta H.$$

Since $y_e > 0$, fluid parcels always move to the south over the topography in this limit. The southward movement is larger than would be predicted from quasi-geostrophic theory which yields $y_i = y_e - f_0 h_0/\beta H$.

The circulation, lift, and blocking can be calculated from the boundary-layer solution, giving

$$L = \pi h_0 \frac{(2-h_0)^2}{4(1-h_0)^2}, \quad \Gamma = -\frac{\pi h_0}{\epsilon b^{\frac{1}{2}}(1-h_0)}, \quad T = -\frac{h_0}{2(1-h_0)}$$

for the finite-depth solution. There is enhanced flow over the topography relative to the background flow so that T is negative. The quasi-geostrophic solution gives $L = \pi h_0$, $\Gamma = -\pi h_0/\epsilon b^{\frac{1}{2}}$, and $T = 0$, the small-h_0 limits of the finite-depth results.

The variation of the solutions with the various parameters in the problem can be understood by considering the global quantities that can be calculated from ψ. The f-plane limit of the circulation is $\pi h_0/\epsilon$ and is the upper limit of the circulation on the β-plane. This is because the β-effect works to compensate the vortex squashing generated over the topography. The magnitude of the quasi-geostrophic circulation is always smaller than the finite-depth circulation (figure 2*a*). The lift in the finite-depth solution is larger than that found from the quasi-geostrophic solution and the f-plane solution (figure 2*b*). The effect of β is to keep the streamlines more nearly aligned with the lines of constant $(f_0+\beta y)/h$, allowing the odd portion of the stream function, ψ_o, to dominate as b is increased. The quadratic terms in the pressure also contribute to the lift in the finite-depth calculation, rectifying the even part of ψ, and contributing to the force on the topography. For small b, the blocking efficiency is larger in the finite-depth model than the quasi-geostrophic model because flow is diverted around the topography and this effect is enhanced as h_0 increases (figure 2*c*). The blocking efficiency is smaller on the β-plane than on the f-plane because the planetary vorticity can compensate the stretching vorticity, allowing fluid parcels to go over the topography more easily. When b becomes larger, the blocking efficiency becomes negative as was demonstrated in the boundary-layer solution.

Johnson (1978) showed that closed streamlines occur less easily for the finite-depth model than for the quasi-geostrophic solution on the f-plane. This is also true on the β-plane. For the quasi-geostrophic model, the critical height for closed streamlines to occur is given by

$$h_{\text{crit}} = \frac{\epsilon}{I_1(b^{\frac{1}{2}})\,K_1(b^{\frac{1}{2}})}, \tag{10}$$

which is found by setting ψ_r to zero, at $\theta = \frac{1}{2}\pi$, $r = 1$. Likewise, in the finite-depth model, the requirement is

$$\frac{1}{1-h_0} + b_1 \kappa I_0'(\kappa) + b_2 \kappa I_1'(\kappa) = 0, \tag{11}$$

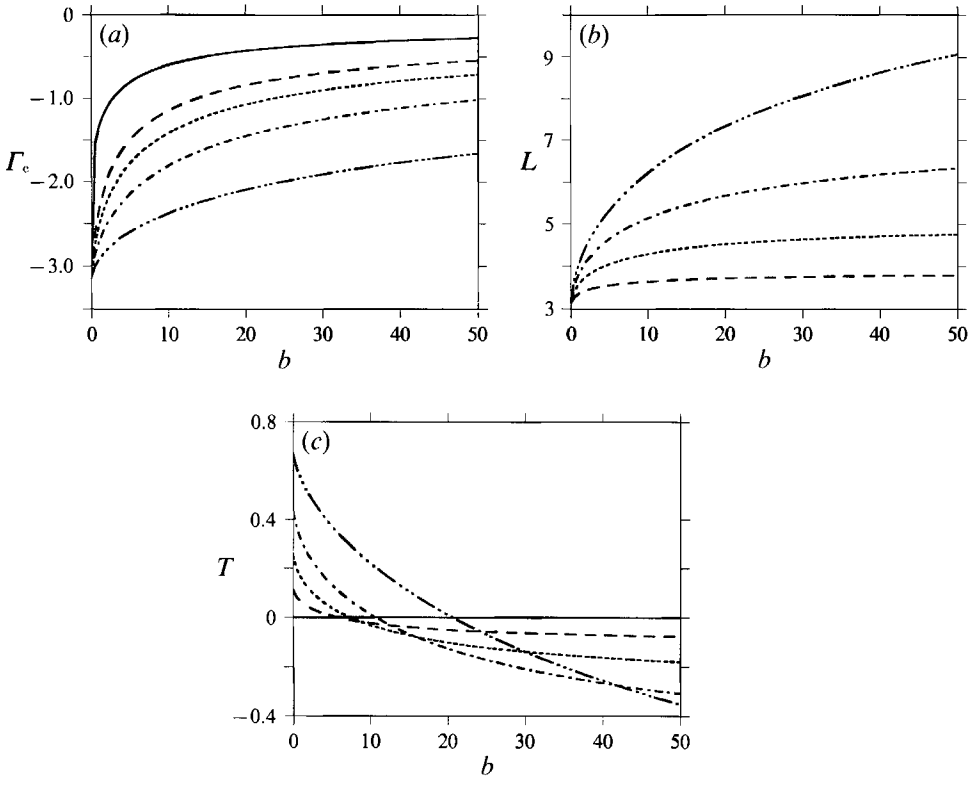

FIGURE 2. Global quantities calculated from the solution for westward flow. Quantities are shown for $h_0 = 0.2$ (long dash line), 0.4 (short dash line), 0.6 (dot-dash line), 0.8 (dash dot-dot-dot line), and the quasi-geostrophic solution (solid line). (*a*) The circulation Γ in units of h_0/ϵ. The circulation is always negative (anticyclonic). (*b*) Lift L in units of h_0. The quasi-geostrophic lift is πh_0. (*c*) Blocking efficiency T. Blocking efficiency for the quasi-geostrophic solution is 0.

where b_1 is proportional to $1/\epsilon$ and both b_1 and b_2 are functions of b and h_0. Note that h_0 appears implicitly in κ. The critical Rossby number above which no closed streamlines exist is found by solving for ϵ in (10) and (11) and letting h_0 go to 1 as the upper limit on the height of the topography. Above this point, the critical height is greater than 1, which is unphysical. Doing this gives

$$\epsilon_{\max} = I_1(b^{\frac{1}{2}})\,K_1(b^{\frac{1}{2}})$$

for the quasi-geostrophic solution and

$$\epsilon_{\max} = \frac{K_1(b^{\frac{1}{2}})}{2(b^{\frac{1}{2}}K_0(b^{\frac{1}{2}}) + 2K_1(b^{\frac{1}{2}}))}$$

for the finite depth solution, where we have substituted in the forms of b_1 and b_2. The f-plane limit of $\frac{1}{4}$ can be found by letting b go to zero. For both solutions, the critical Rossby number is a monotonically decreasing function of b that approaches zero as $b \to \infty$; in this limit, the β-effect inhibits north–south movement of streamlines. The maximum Rossby number is always larger for the quasi-geostrophic model, indicating that it is harder to form closed streamlines in the finite-depth model.

2.3. *Solutions for eastward flow on the β-plane*

For eastward flow lee Rossby waves are formed downstream of the topography. McCartney (1975) found the quasi-geostrophic solution applying the boundary condition (7):

$$\psi = r\sin\theta + \frac{2h_0}{\epsilon b^{\frac{1}{2}}} J_1(b^{\frac{1}{2}})\, S(b^{\frac{1}{2}}r,\theta) - \frac{h_0}{\epsilon b^{\frac{1}{2}}}\{\tfrac{1}{2}\pi S(b^{\frac{1}{2}}r,\theta)\, J_1(b^{\frac{1}{2}})\, Y_0(b^{\frac{1}{2}}r)\} \quad \text{for} \quad r > 1$$

and

$$\psi = r\sin\theta + \frac{2h_0}{\epsilon b^{\frac{1}{2}}} J_1(b^{\frac{1}{2}})\, S(b^{\frac{1}{2}}r,\theta) - \frac{h_0}{\epsilon b^{\frac{1}{2}}}\left\{\tfrac{1}{2}\pi\, Y_1(b^{\frac{1}{2}})\, J_0(b^{\frac{1}{2}}r) + \frac{1}{b^{\frac{1}{2}}}\right\} \quad \text{for} \quad r < 1,$$

where

$$S(\xi,\eta) = \sum_{n=1}^{\infty}\left[\frac{J_{2n-1}(\xi)\cos((2n-1)\eta)}{2n-1}\right].$$

For the finite-depth problem, the matching conditions require that the solution contain odd (sine) wave modes in addition to the even (cosine) wave modes. We use the approach that Miles & Huppert (1968) developed to find the solution in an analogous system of flow in a stratified fluid over a semi-circular obstacle. They constructed lee wave functions that satisfied the boundary condition individually. They required functions that were odd in y, so we extend their work to include the even modes.

The lee wave functions are constructed such that they each satisfy the boundary condition asymptotically and are given by

$$\delta_n^{\mathrm{o}}(r,\theta) = Y_n(b^{\frac{1}{2}}r)\sin n\theta + \phi_n^{\mathrm{o}}(r,\theta)$$

for the odd functions and

$$\delta_n^{\mathrm{e}}(r,\theta) = Y_n(b^{\frac{1}{2}}r)\cos n\theta + \phi_n^{\mathrm{e}}(r,\theta)$$

for the even functions, where

$$\phi_n^{\mathrm{o}}(r,\theta) = \sum_{q=1}^{\infty} J_q(b^{\frac{1}{2}}r)\sin q\theta$$

and

$$\phi_n^{\mathrm{e}}(r,\theta) = \sum_{q=1}^{\infty} J_q(b^{\frac{1}{2}}r)\cos q\theta.$$

The finite-depth solution for $r > 1$ can be written as a sum over the lee wave functions, and by changing the order of summation,

$$\psi = -r\sin\theta + \sum_{n=0}^{\infty}\left\{\left[\sum_{q=1}^{\infty} a_q Z_{nq}(b^{\frac{1}{2}}r)\right]\sin n\theta + \left[\sum_{q=0}^{\infty} c_q X_{nq}(b^{\frac{1}{2}}r)\right]\cos n\theta\right\}$$

and

$$Z_{nq} = \delta_{nq}\, Y_n(b^{\frac{1}{2}}r) + b_{qn}\, J_n(b^{\frac{1}{2}}r), \quad X_{nq} = \delta_{nq}\, Y_n(b^{\frac{1}{2}}r) + d_{qn}\, J(b^{\frac{1}{2}}r),$$

where

$$b_{kl} = \begin{cases} (4/\pi)\,k/(l^2-k^2), & k \text{ even}, l \text{ odd} \\ (4/\pi)\,l/(l^2-k^2), & k \text{ odd}, l \text{ even} \\ 0, & k-l \text{ even} \end{cases}$$

and

$$d_{kl} = \begin{cases} (4/\pi)\,l/(l^2-k^2), & k \text{ even}, l \text{ odd} \\ (4/\pi)\,k/(l^2-k^2), & k \text{ odd}, l \text{ even} \\ 0, & k-l \text{ even} \\ (4/\pi)\,1/l, & k = 0, l \text{ odd} \\ -(2/\pi)\,1/k, & k \text{ odd}, l = 0. \end{cases}$$

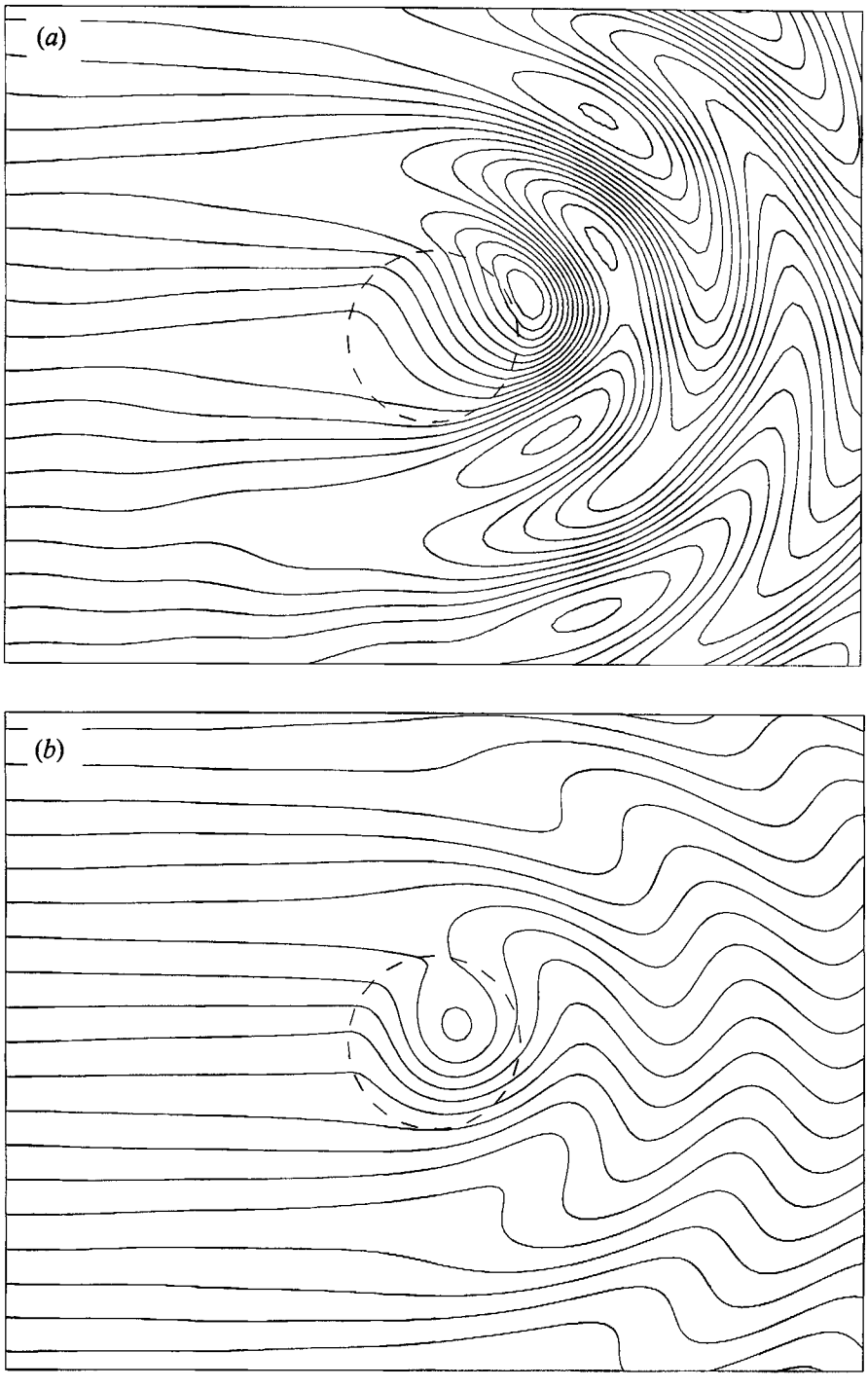

FIGURE 3. Stream function for eastward flow when $b = 10$, $h_0 = 0.5$ and $\epsilon = 0.1$. (*a*) Finite-depth solution, and (*b*) quasi-geostrophic solution.

Here δ_{ij} is the Kronecker delta. For $r < 1$ the solution is

$$\psi = -\frac{r\sin\theta}{1-h_0} - F_0 + \sum_{n=0}^{\infty} J_n(k_2 r)[b_n \sin n\theta + d_n \cos n\theta]. \tag{12}$$

Applying the matching conditions gives an infinite set of coupled linear equations. They comprise two sets of equations for a_q and b_n and two sets of equations for c_q and d_n. In order to solve these, n and q are truncated at N, and then the set of equations is solved numerically. We let $N = 10$, and it can be seen in the solutions constructed below that the upstream waves are small, showing that the upstream boundary condition is satisfied asymptotically.

Once again, in the limit of large b, the finite-depth and quasi-geostrophic solutions are very different (figure 3). In this case, we cannot construct a simple boundary-layer solution as we did for westward flow because large-amplitude lee Rossby waves are generated. For the finite-depth model, the stationary Rossby waves generated over the topography have very large amplitude as they compensate for the large amount of relative vorticity generated. Although these waves may not be stable, and would certainly be modified by frictional effects, the solutions show that large-amplitude Rossby waves could be generated that are not predicted from the quasi-geostrophic solution.

We proceed to calculate the circulation, lift and blocking as for the westward flow solutions. The circulation for the quasi-geostrophic solution is

$$\Gamma = 2\pi(h_0/\epsilon) J_1(b^{\frac{1}{2}}) Y_1(b^{\frac{1}{2}}),$$

while the circulation for the finite-depth model is shown graphically (figure 4*a*). The magnitude of the circulation oscillates with a wavenumber of approximately $b^{\frac{1}{2}}(1-h_0)$, the wavenumber of the variations over the topography. The circulation reverses sign owing to local reversals of direction in the wave pattern which is illustrated in figure 3. The blocking efficiency becomes negative for large b as it did for the westward flow (figure 4*b*). This results from the same tendency for the streamlines to follow lines of constant planetary vorticity when b is large so that the flow is enhanced over the topography. However, this trend does not continue indefinitely, because eventually the wave field has large enough amplitude and small enough wavelength to dramatically affect the flow immediately over the topography. The lift increases with increasing h_0, and is greater than that found on the f-plane or for the quasi-geostrophic solution (figure 4*c*). This effect was also seen for westward flow; the odd portion of the wave function tends to dominate as b increases since quadratic terms in the pressure rectify the lee wave signal in the lift.

The drag from the quasi-geostrophic solution is given by

$$D = 2\pi\epsilon(h_0/\epsilon)^2 J_1^2(b^{\frac{1}{2}})/b^{\frac{1}{2}}.$$

The resulting drag has zeros in it, associated with the resonant solutions as discussed by McCartney (1975). The envelope of the curve decays with increasing b, decreasing algebraically as b^{-1}. As shown by Johnson (1977), the wave drag associated with eastward flow over topography depends critically on the form of the topography, and the resonant solutions do not appear for flow over smooth topography. However, the qualitative comparisons between the finite-depth and quasi-geostrophic theory should still be valid for similar solutions of flow over smooth topography. The drag in the finite-depth model is composed of two parts, one due to the part of P_e proportional to $1/\epsilon$ and the other to the part proportional to ϵ (figure 5). The first part of the drag has

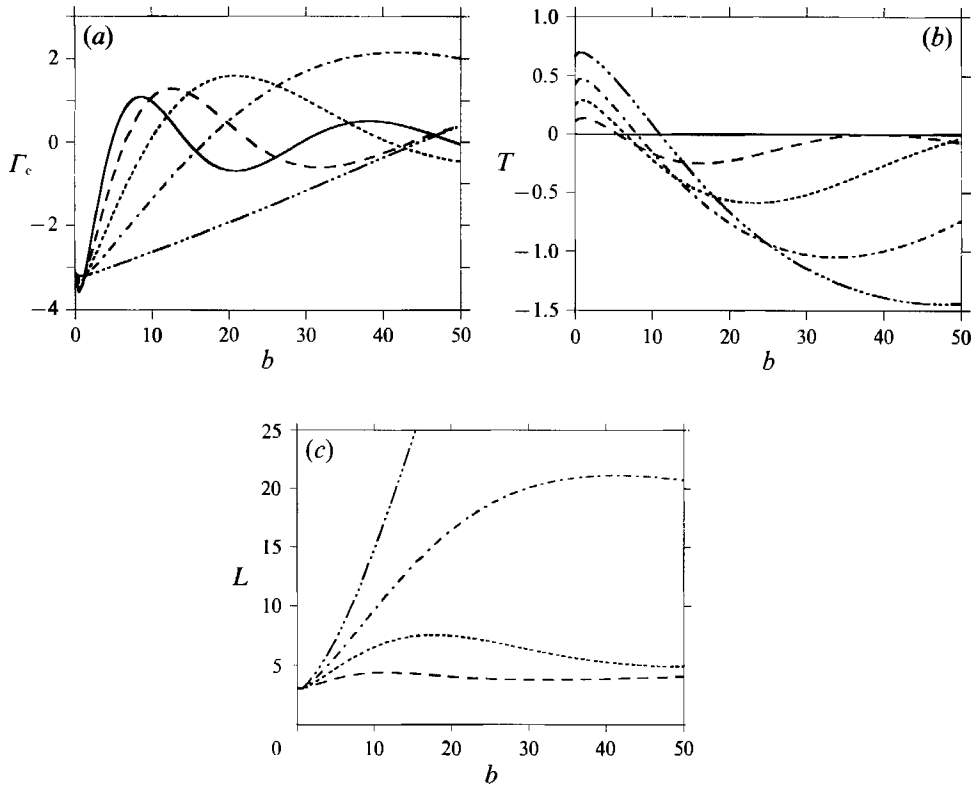

FIGURE 4. Global quantities calculated from the solution for eastward flow. Quantities are shown for $h_0 = 0.2$ (long dash line), 0.4 (short dash line), 0.6 (dot-dash line), 0.8 (dash dot-dot-dot- line), and the quasi-geostrophic solution (solid line). (*a*) Circulation Γ in units of h_0/ϵ. (*b*) Blocking efficiency T. Blocking efficiency for the quasi-geostrophic solution in 0. (*c*) Lift L in units of h_0. The quasi-geostrophic lift is πh_0.

size comparable to the quasi-geostrophic drag, while the other part increases dramatically for increasing h_0. The second component does not contribute when $\epsilon \to 0$, but even for relatively small Rossby numbers (for instance $\epsilon = 0.1$) it can be very large owing to the large-amplitude Rossby waves generated downstream when both b and h_0 are large (figure 5*c*). Thus, the drag calculated from the finite-depth model has a very different character than that from the quasi-geostrophic model. The part of the pressure that contributes to the drag, P_e, has quadratic dependence on the stream function so that the large-amplitude downstream wave field contributes a large amount to the drag.

2.4. *Discussion*

Quasi-geostrophic theory tends to underestimate the strength of the flow over the topography, resulting in an underestimate of the lift and drag and an overestimate of the circulation of the flow. In addition, the quasi-geostrophic approximation results in a critical Rossby number (above which closed streamlines cannot exist above the topography) which is too large. The steady solutions discussed here may not be realizable in practice. In the laboratory (Boyer *et al.* 1984) the flows tend to become unsteady when the Rossby number increases. There have been no laboratory experiments where the β-effect is very strong $b \gg 1$; however, the large-amplitude lee waves generated downstream of the topography when b is large may modify the

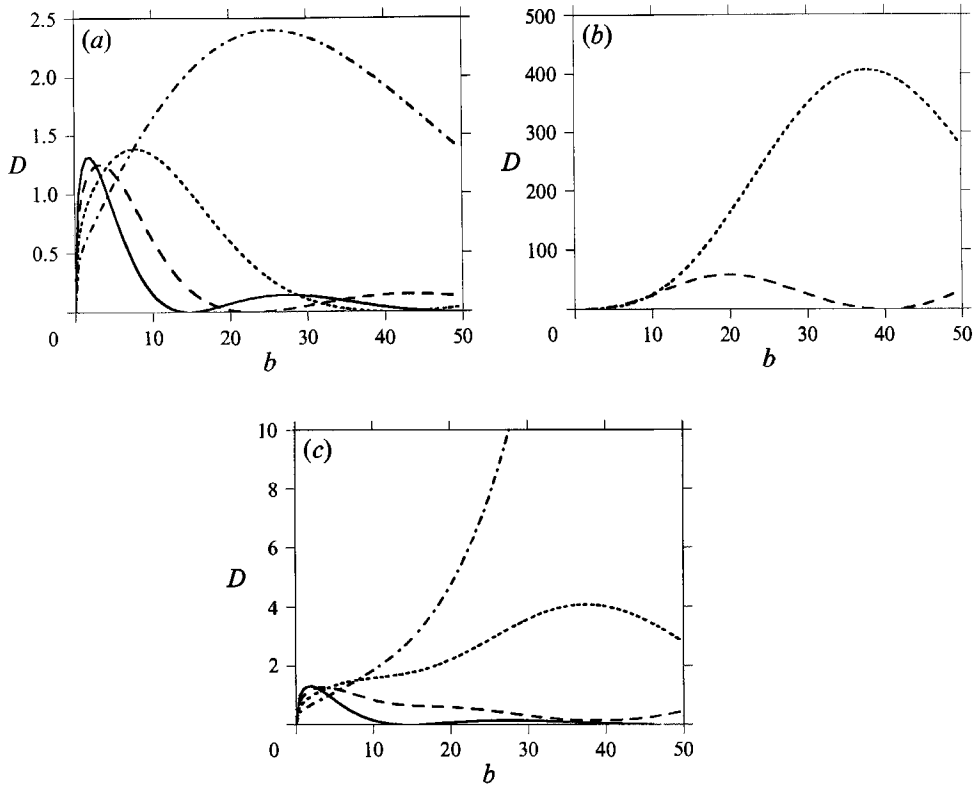

FIGURE 5. Drag D for eastward flow as a function of b. Shown for $h_0 = 0.2$ (long dash line), 0.4 (short dash line), 0.6 (dash-dot line), and quasi-geostrophic solution (solid line). (*a*) The portion proportional to $1/\epsilon$ in units of h_0^3/ϵ. (*b*) The portion proportional to ϵ in units of $h_0^2\epsilon$; $h_0 = 0.6$ is not shown because it is off the scale of the plot. The quasi-geostrophic contribution is zero. (*c*) Drag with $\epsilon = 0.1$ in units of h_0^2/ϵ.

upstream condition such that the mean flow would be modified. In addition, the lee waves may become barotropically unstable, making a steady solution unlikely.

3. The initial value problem on the *f*-plane

To investigate time-dependence, we consider the initial value problem of flow impinging on finite topography on the *f*-plane, and for simplicity, we ignore the β-effect. The geometry of a right-circular cylinder allows the use of the method of contour dynamics. The method is modified to implement the matching conditions on the edge of the topography. The validity of the quasi-geostrophic approximation is also investigated in this context.

3.1. *The quasi-geostrophic initial value problem*

Koslov (1983) used contour dynamics to study the quasi-geostrophic initial value problem, and we begin by reviewing his results. In a barotropic rotating fluid, the potential vorticity is advected by the stream function. The evolution of the fluid can be described by the potential vorticity equation (2). The stream function can be calculated using a Green's function,

$$\psi(x,y) = \int\int q(\xi,\eta)\, G(x,x',y,y')\, \mathrm{d}x'\, \mathrm{d}y' + \text{boundary contributions} \qquad (13)$$

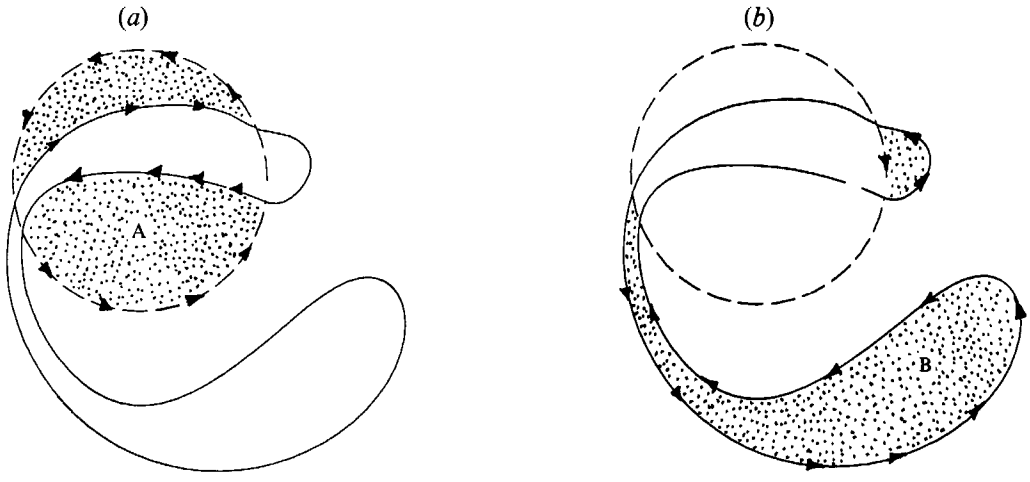

FIGURE 6. Schematic of the different regions of constant relative vorticity. Outside of the contours, the vorticity is zero. (*a*) The stippled region has negative relative vorticity (region A), and (*b*) the stippled region has positive relative vorticity (region B). The arrows indicate direction of integration. Areas which are not stippled in either (*a*) or (*b*) have zero relative vorticity. For the quasi-geostrophic model, the two values of non-zero vorticity exactly cancel, and the integration can instead be done over the circle and the deformed contour. For the finite-depth model, the two regions ($r < 1$ and $r > 1$) must be evaluated separately.

if the potential vorticity q and the boundary conditions are known. For Laplace's equation in a domain with no boundaries, the Green's function takes the simple form

$$G(x, x', y, y') = (1/2\pi) \ln R, \tag{14}$$

where $R = [(x-x')^2 + (y-y')^2)]^{\frac{1}{2}}$. If h is piecewise constant, the relative vorticity is zero initially, and q is conserved; then q will be piecewise constant so that it can be taken out of the integral. In order to calculate the velocity at any point, we differentiate (13) with respect to x and y, invoke the symmetry of the Green's function, and use Green's theorem to obtain

$$(u, v) = (-\partial_y \psi, \partial_x \psi) = q \oint_{\partial D} G(R)(\mathrm{d}x', \mathrm{d}y'). \tag{15}$$

The velocity at any point is found by evaluating the contour integral. In order to find the evolution of the flow field, the evolution of ∂D must be known, and it can be found by calculating the velocity on ∂D.

This method reduces the problem of solving for the nonlinear evolution of the field to that of evaluating (15) at each time step. Once the velocity on ∂D is known, it can be stepped forward in time to find the new location of the contour. The implementation of this technique used here is described in Polvani (1988). At each time step, the boundary of the region of constant relative vorticity is stepped forward via Runge–Kutta integration. The Green's function is singular on the contour, but the singularity can be handled by using the method in Polvani's Appendix B. The basic contour dynamics computer code was developed by Meacham (1991). As the contour deforms with time, the distances between the points on the contour change, and an adjustment in the spacing of the points on the contour is made to carry the calculation forward in time accurately. The points are redistributed according to the local rate of curvature and are added or removed as needed, and when the contour comes back on

itself, it is pinched off. Only when many (on the order of 10) pinch-offs have occurred is there a significant loss of vorticity (on the order of 1%) in any of the calculations in this study.

After the background flow has been turned on, there are two regions of non-zero vorticity to consider (figure 6). The region of fluid which originated upstream that moves over the topography (the stippled region in figure 6*a*, region A) has relative vorticity $-h_0/\epsilon$; the region of fluid which originated over the topography that moves off the topography (the stippled region in figure 6*b*, region B) has relative vorticity h_0/ϵ. In order to find the flow everywhere, a contour integral around region A and B must be evaluated. Instead of evaluating the contours that bound the regions A and B separately, we evaluate the topographic contour (a circle) using potential vorticity $-h_0/\epsilon$ and the contour that bounds the fluid that originated over the topography using potential vorticity h_0/ϵ and add the results to take advantage of the cancellation in the zero-vorticity region. This method can be used for an arbitrarily shaped region and is not restricted to a circle. Koslov (1983) considered flow over a circular cylinder, where an analytic solution can be found for the topographic contour integral.

We demonstrate the two dynamical regimes that Huppert & Bryan (1976) first observed. When the topography is small (figure 7*a*) all of the fluid which originates over the topography is swept downstream by the background flow and assumes a tear-drop shape as it is influenced by the anticyclonic circulation over the topography. When the topography is tall some of the fluid that originates over the topography remains trapped there (figure 7*b*). In this example, initially the fluid which originated over the topography is pushed downstream. It then moves clockwise around the topography in response to the anticyclonic vorticity. The upper part of the contour is advected over the top of the bump, while the lower part is stretched downstream, giving the C-shape. Finally, the upper part of the C is advected to the south and clockwise around the topography while the lower part of the C is shed downstream. Eventually the calculation must be stopped because the contours become too broken up. To supplement Kozlov (1983), we show the velocity field so that dipole structure of the flow is easily seen (figure 8). The subsequent advection of the blob of fluid which originated over the topography can be observed, as well as the cyclonic vortex which is shed downstream.

Verron & Le Provost (1985) noticed that when the fluid has been moved to the base of the topography (for instance see $t = 1$ in figure 7*b*) it appears to be in a state similar to the steady-state solution found by Johnson (1978) using variational techniques. However, the flow progressively alters after this point. In the quasi-geostrophic solutions that Johnson presented, the contour of positive potential vorticity does not overlap the topography, unlike the example shown here, although the parameter value used here lies in the regions where Johnson (1978) found steady solutions (in Johnson's notation, $\alpha = 0.2$ for the example in figure 7*b*). We observe progressive ejection of filaments from the patch of fluid that originated over the topography as the fluid is advected clockwise around the topography. A linear wave oscillates around the topography in a period $t = 4\pi\epsilon/h_0$, 2.5 for the example shown (Johnson 1984). The period of rotation in our simulation is approximately 4. The discrepancy between the numerical model and linear theory is due to the ejection of vorticity away from the topography. In the results of Verron & Le Provost (1985) and James (1980), ejected fluid is often entrained back into the trapped fluid. This process is enhanced by the presence of friction.

It is plausible that the system reaches a quasi-steady state with a finite amount of fluid trapped over the topography for a timescale long compared to an advection

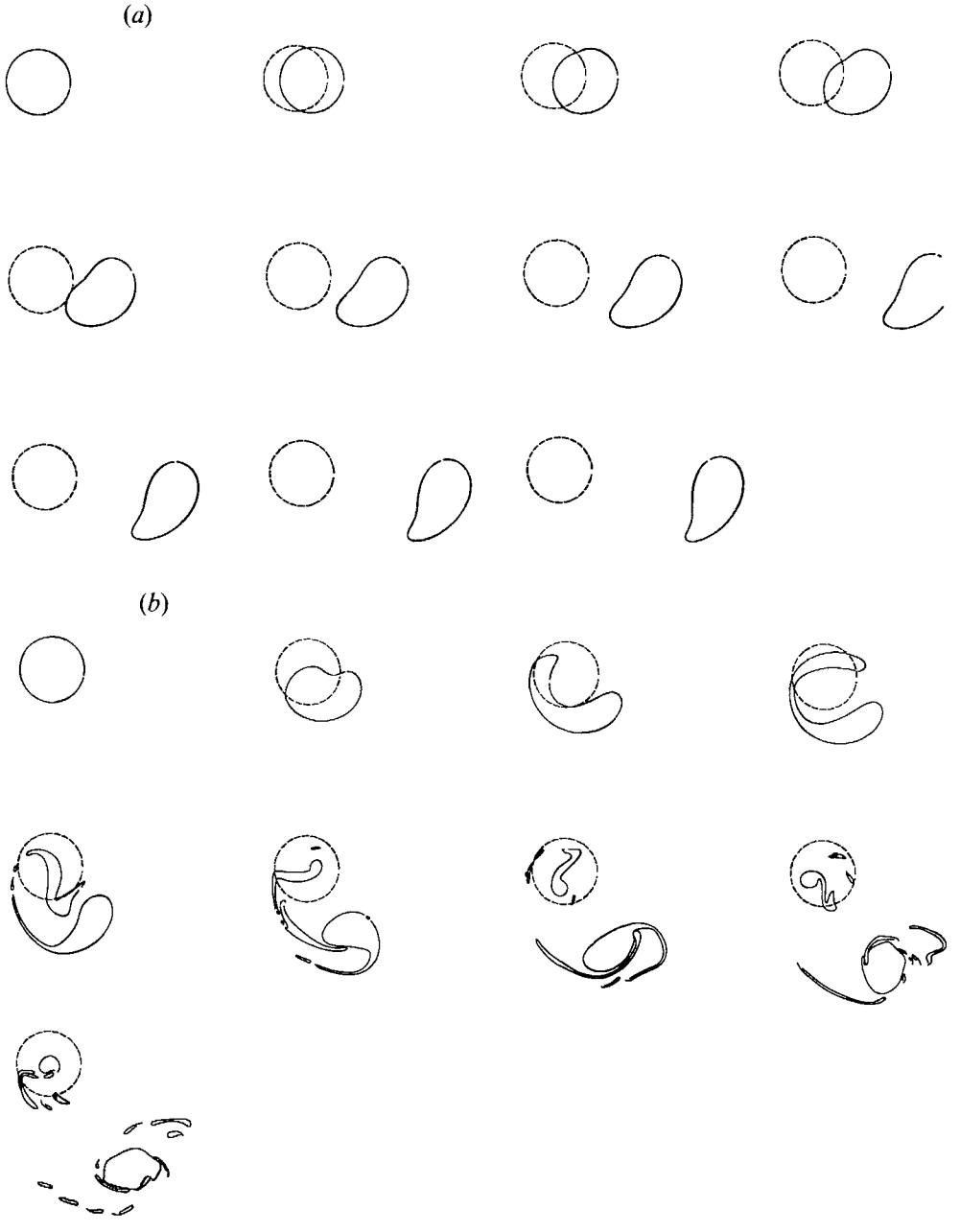

FIGURE 7. Time evolution of the contour that delineates fluid which originated over the topography after the background flow has been turned on abruptly at $t = 0$. A snapshot of the contours is taken at $t = 0, 1, \ldots, 9$ with time increasing to the right and downward. The dashed contour is the boundary of the topography; the solid contour delineates the boundary of the fluid that originated over the topography. (*a*) $h_0/\epsilon = 1$, and (*b*) $h_0/\epsilon = 5$.

timescale yet short compared to the spindown time of the fluid. Vorticity ejection and entrainment is probably an important mechanism in the path to the steady state. Unfortunately, the numerics become invalid before a steady-state solution is reached. However, we can explore the approach to different possible steady-state solutions.

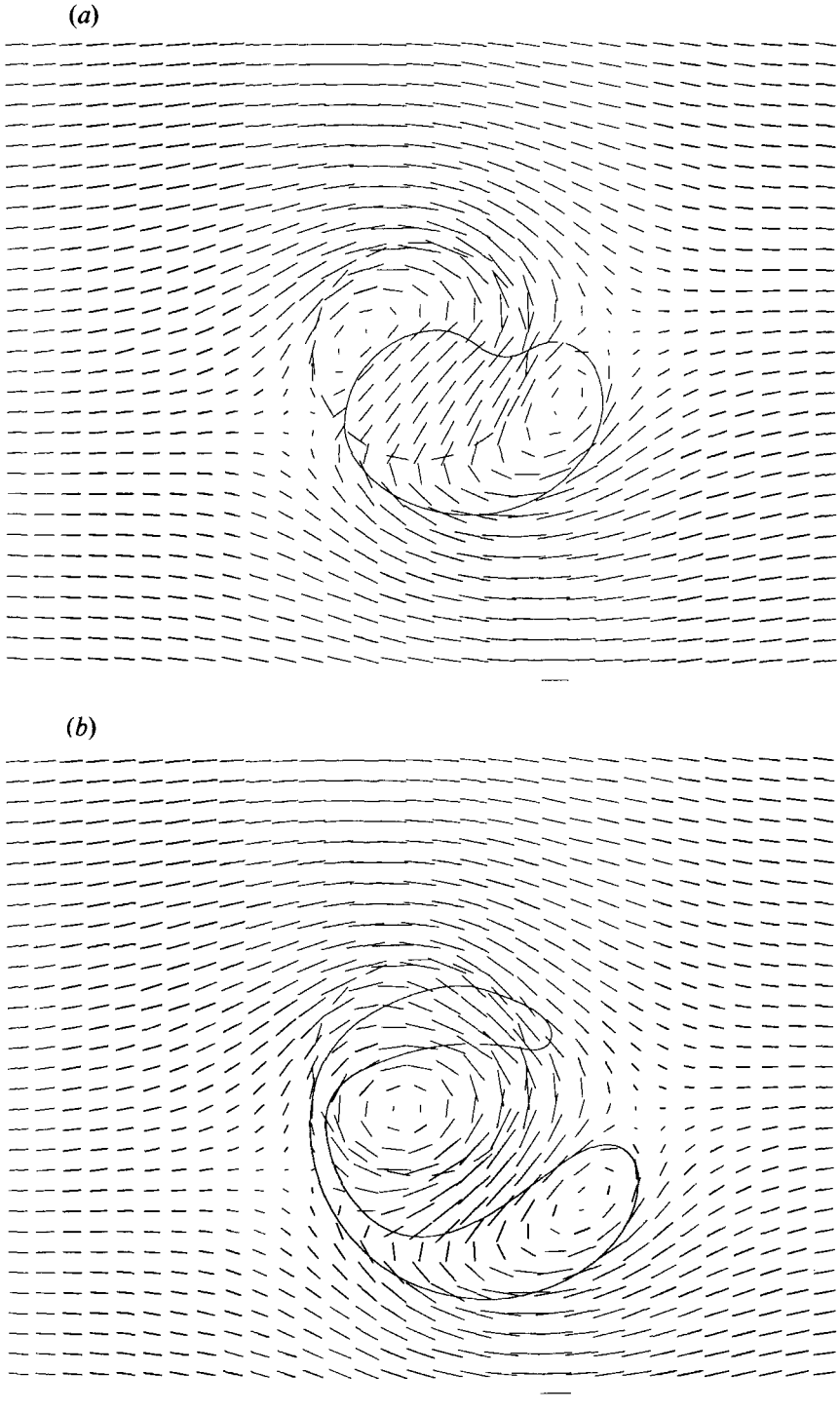

FIGURE 8(a,b). For caption see facing page.

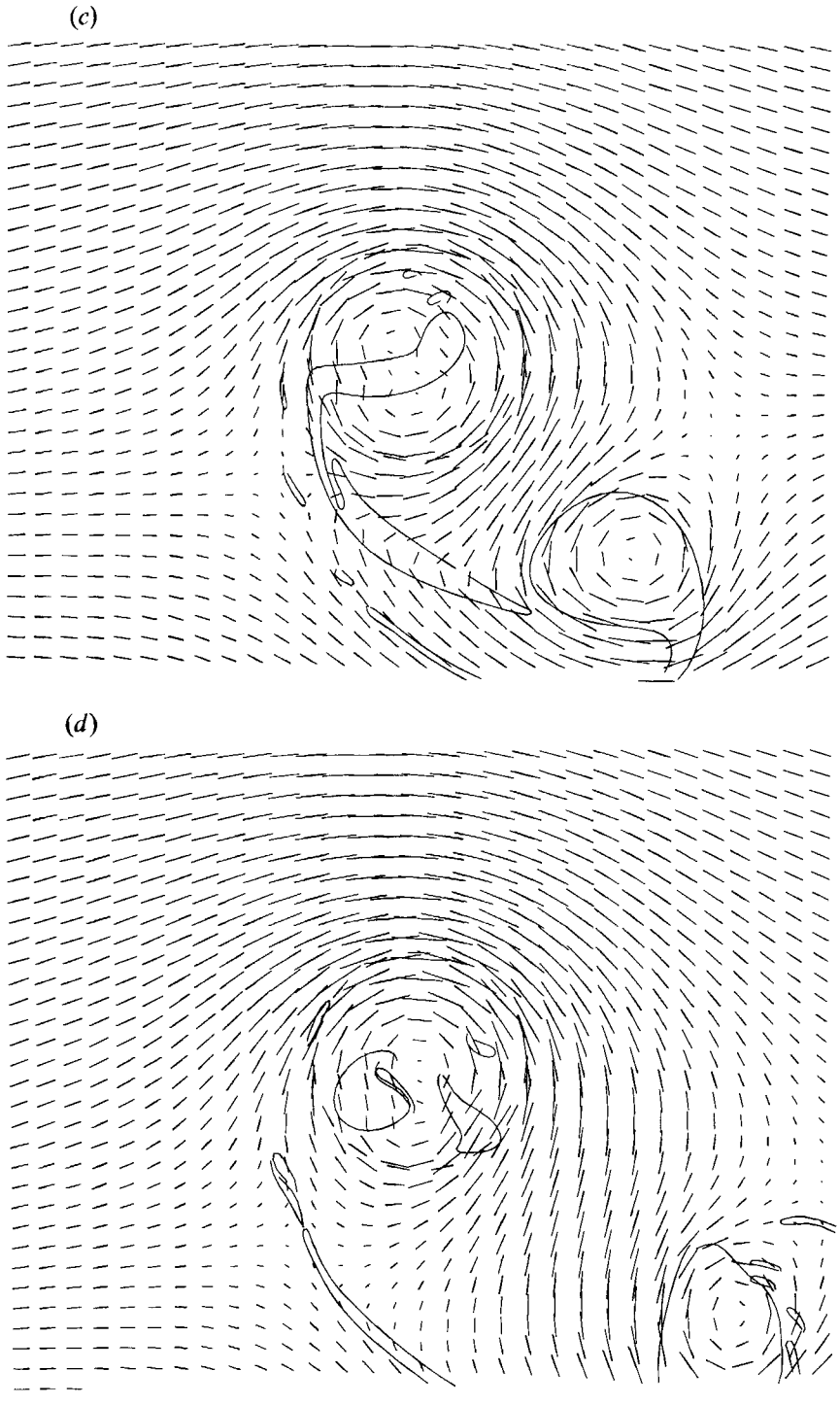

FIGURE 8. Velocity field for the case in figure 7(*b*) at (*a*) $t = 1$, (*b*) $t = 3$, (*c*) $t = 5$, and (*d*) $t = 7$. The background flow goes from left to right.

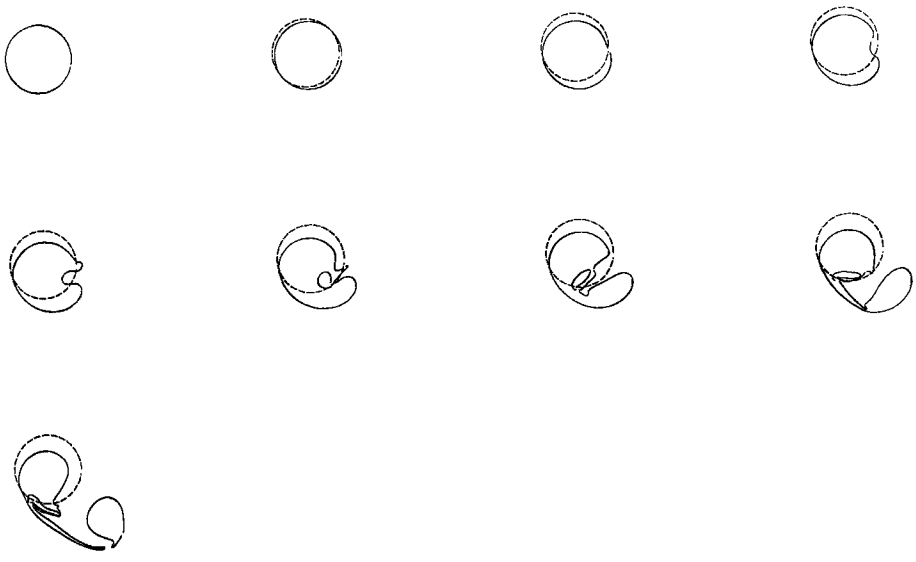

FIGURE 9. Time evolution of the contour for a case when the background flow is turned on slowly with timescale $\tau = 4$ and $h_0/\epsilon = 5$. A snapshot of the contours is taken at $t = 0, 1, \ldots, 8$.

First, we explore if time-dependence in the background flow can change the final state of the system. We choose

$$U = U_0 \tanh(t/\tau)$$

as Huppert & Bryan (1976) did. When the background flow is turned on more slowly than in figure 7(*b*), more fluid remains trapped on the topography (figure 9). This suggests that the steady-state solution of the system would be different when the background flow is turned on slowly than when it is turned on abruptly. Johnson (1984) constructed steady solutions such that the maximum amount of fluid possible is retained over the topography. From the results of varying τ, it seems plausible that this solution would be reached were the background flow to be turned on very slowly.

Another possible steady solution, an intermediate retention solution where an intermediate amount of fluid is retained over the topography, provides an infinite set of steady solutions to the inviscid problem. In these solutions, the trapped fluid is contained within a circular contour with centre $x = 0$, $y = 2\epsilon/h_0$ and radius r_0 that has magnitude anywhere from zero up to Ingersoll's (1969) solution radius of $r_0 = r_c = 1 - 2\epsilon/h_0$. The difference between these solutions and Ingersoll's (1969) solutions is that there are closed streamlines located outside the circle of radius r_0 and these closed streamlines trap fluid that originated upstream, but the fluid within the closed streamlines is not spun down through the effects of bottom drag. The family of solutions are given by

$$\psi = -r\sin\theta + \frac{K}{2\pi}\ln\frac{r'}{r_0} - \frac{h_0}{2\epsilon}\begin{cases}\ln r, & r > 1\\ \frac{1}{2}(r^2-1), & r < 1,\end{cases}$$

where $K = \pi h_0 r_0^2/\epsilon$ and r' is the radius referenced to $x = 0$, $y = -2\epsilon/h_0$. The fluid is stagnant within the circle of radius r_0. We numerically tested the stability of this solution to small perturbations and it is stable.

Three possible steady solutions are shown for the parameters used in figure 7*b*: the inertial solution; the intermediate retention solution; and the maximum retention

solution (figure 10). In the inertial solution, all of the fluid which originated over the topography is swept downstream. The intermediate retention solution is constructed such that the amount of fluid trapped over the topography is the same as found in the example shown in figure 7(*b*) in the last time step. This solution resembles the initial value problem results best. The physical reason why different steady states are possible can be understood by considering how the initial value problem progresses. When the background flow is turned on very slowly, one can think of the process as a succession of steady states. The initial steady state is one where there is no flow, and all of the fluid is trapped over the topography. As the background flow increases, the maximum retention solution holds at each instant, so that the final steady state is the maximum retention solution. When the background flow is turned on abruptly however, the fluid moves off the topography before it has time to respond to the anticyclonic flow, loosing some of the fluid necessary to form the maximum retention solution.

3.2. *The finite-depth initial value problem*

For the finite-depth initial value problem, a modified contour dynamics method is used to find the time-dependent behaviour of the system. Since the transport normal to the boundary and the tangential velocity along the topography are both continuous, the Green's function is more complicated than (14) and was given by Johnson (1978). Given the Green's function, the velocity field could be found everywhere. Unfortunately, it lacks the appropriate symmetry needed to apply contour dynamics, and the velocity cannot be determined by evaluating contour integrals. The area integrals can only be transformed into contour integrals as long as the Green's function is composed of a linear combination of functions g_i, with

$$\frac{\partial g_i(\boldsymbol{x}, \boldsymbol{x}')}{\partial x} = \pm \frac{\partial g_i(\boldsymbol{x}, \boldsymbol{x}')}{\partial x'}$$

for each g_i. The same condition must hold for the y and y' derivatives. For Johnson's Green's function, these symmetry conditions do not hold, and the problem is solved by applying the matching conditions explicitly at each time step.

Before the background flow has been turned on, the upstream fluid has potential vorticity $q = 1$ while the potential vorticity of the fluid over the topography has value $q = 1/(1-h_0)$. When the background flow is turned on, the fluid over the topography is pushed off and stretched, gaining cyclonic relative vorticity

$$\zeta = \frac{h_0}{\epsilon(1-h_0)}, \tag{16}$$

while the fluid that has been brought from upstream over the topography now has anticyclonic relative vorticity

$$\zeta = -\frac{h_0(1-h_0)}{\epsilon}. \tag{17}$$

In the quasi-geostrophic limit, $h_0 \to 0$ but h_0/ϵ finite, we find that (16) and (17) have the same magnitude.

The problem is solved at each time step by considering the region $r > 1$ separately from the region $r < 1$. The velocity field is found for $r > 1$ by assuming that the only sources of vorticity in the problem are those located at $r > 1$ (i.e. the stippled region in figure 6*b*). Likewise, the velocity field for $r > 1$ is found using only those sources located at $r < 1$ (i.e. the stippled region in figure 6*b*). The logarithmic barotropic

(a)

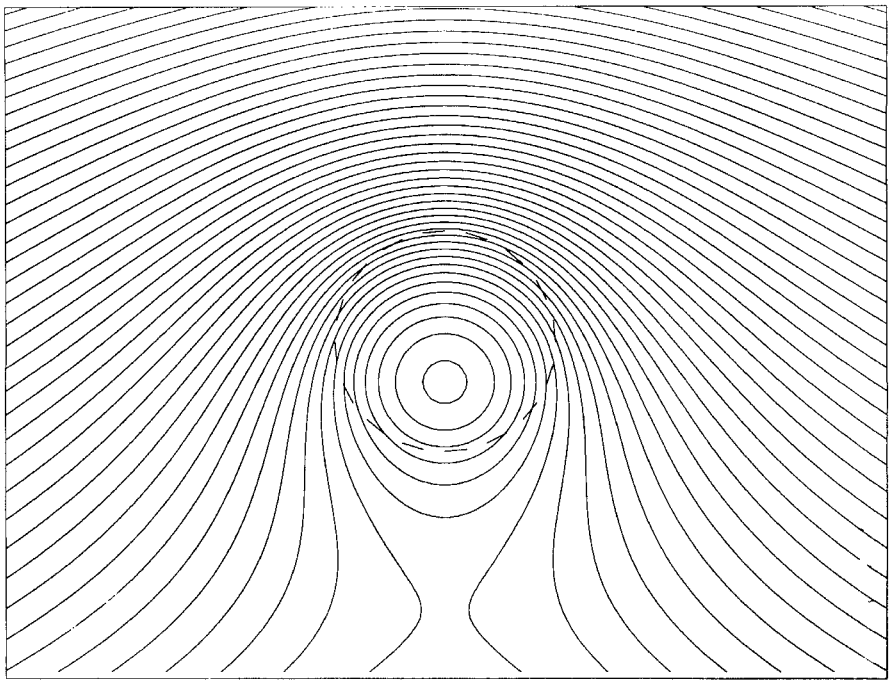

(b)

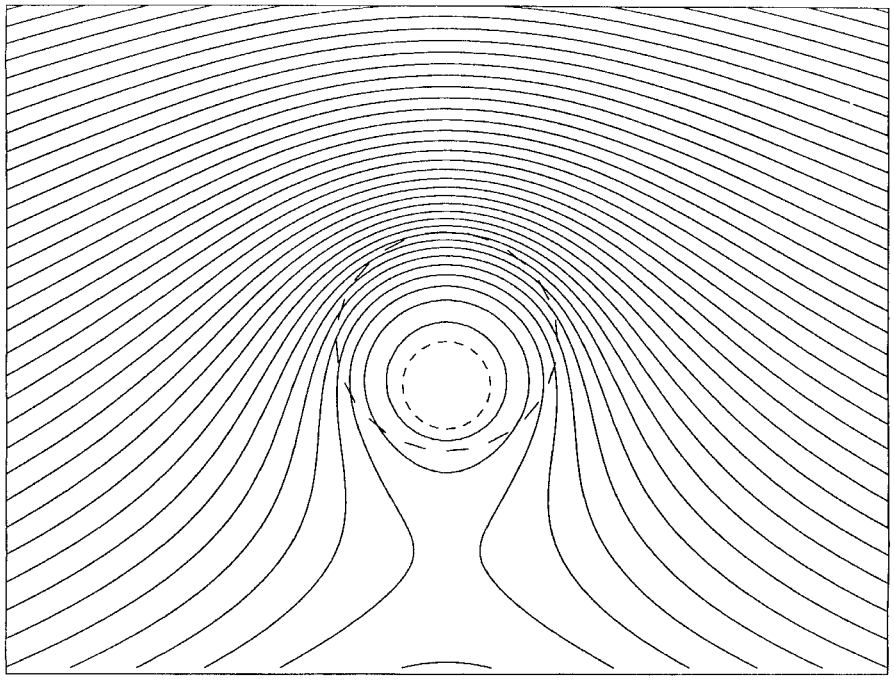

FIGURE 10(a,b). For caption see facing page.

(*c*)

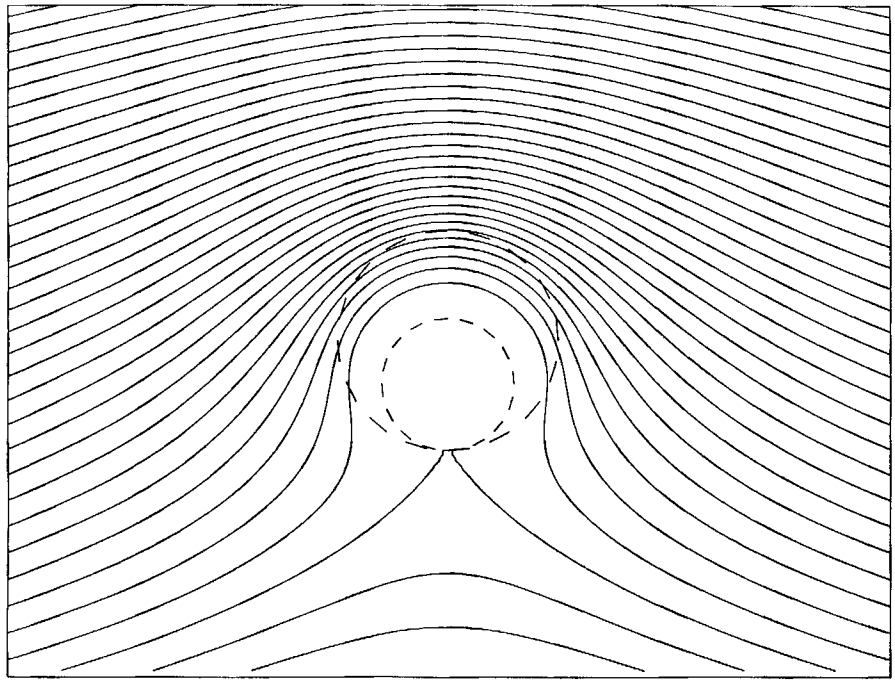

FIGURE 10. Streamlines for steady inviscid flow over topography when $h_0/\epsilon = 5$. (*a*) The inertial solution $\psi^{(a)}$, (*b*) the intermediate retention solution with $r_0 = 0.4$ and (*c*) Ingersoll's (1969) solution.

Green's function is used in each case. In order match the two regions together, a homogeneous (zero vorticity) solution is constructed. To do this, the velocity at $r = 1$ is calculated at $2^m = N$ points evenly spaced in θ from the two cases discussed above (i.e. at $r = 1^+$ and $r = 1^-$).

These velocities are transformed to polar coordinates via

$$\hat{r} = \hat{\imath}\cos\theta + \hat{\jmath}\sin\theta, \quad \hat{\theta} = -\hat{\imath}\sin\theta + \hat{\jmath}\cos\theta,$$

and

$$\hat{\imath} = \hat{r}\cos\theta - \hat{\theta}\sin\theta, \quad \hat{\jmath} = \hat{r}\sin\theta + \hat{\theta}\cos\theta$$

since the matching conditions are applied to the radial and azimuthal velocities. A fast Fourier transform is performed on the polar velocities at $r = 1$ to decompose them into modes in θ such that

$$u(r = 1^-, \theta) = \sum_{n=-N/2}^{N/2} u_n^{(\mathrm{i})} \mathrm{e}^{-\mathrm{i}n\theta}$$

and

$$v(r = 1^-, \theta) = \sum_{n=-N/2}^{N/2} v_n^{(\mathrm{i})} \mathrm{e}^{-\mathrm{i}n\theta},$$

where u is now the radial velocity and v the azimuthal velocity. Likewise, similar equations can be written with superscripts o instead of i for the velocity at $r = 1^+$.

To match the two regions together, a homogeneous series solution to Laplace's equation is added. The homogeneous (zero vorticity) solution can be written

$$\psi_{\mathrm{h}}^{(\mathrm{i})} = \sum_{-\infty}^{\infty} a_n \mathrm{e}^{-\mathrm{i}n\theta} r^{|n|} \quad \text{for} \quad r < 1 \tag{18}$$

and $$\psi_{\mathrm{h}}^{(\mathrm{o})} = \sum_{-\infty}^{\infty} b_n \mathrm{e}^{-\mathrm{i}n\theta} r^{-|n|} + b \ln r \quad \text{for} \quad r > 1. \tag{19}$$

The contribution to the velocity from the homogeneous solutions is found by taking the appropriate derivatives in r and θ.

The matching conditions then reduce to

$$\mathrm{i}na_n + (1-h_0)\, u_n^{(\mathrm{i})} = \mathrm{i}nb_n + u_n^{(\mathrm{o})} \tag{20}$$

for the transport normal to the edge of the topography to be continuous, and

$$\frac{na_n}{1-h_0} + v_n^{(\mathrm{i})} = -nb_n + v_n^{(\mathrm{o})} + b\delta_{n,0} \tag{21}$$

for the tangential velocity to be continuous. From (20) and (21), the coefficients a_n and b_n in (18) and (19) can be calculated. For a real solution $a_n = a_{-n}^*$ and $b_n = b_{-n}^*$.

To find the velocity field, the contour integral is calculated for either region A or B and the series solution is found for the location in question. Typically 16 modes are used in the decomposition. Mass is conserved, as long as the contours are not too broken up, so that the method of applying the matching conditions does not affect the accuracy of the solution. Note that vorticity and mass conservation no longer implies area conservation; rather the depth-weighted area is conserved.

The contour integrals themselves are more difficult to evaluate than those in the quasi-geostrophic problem where the cancellation in the zero-vorticity region can be taken advantage of. The algorithm used to calculate each line integral consists of several steps. First, the intersection points of the contour with the edge of the topography (the circle of radius 1) are found. Whether the contour is entering or exciting the circle, in the sense of the direction of the integration, is recorded as a vector. Then the intersection points and flags are ordered in θ. For the part of the integral on the movable contour, the integration is done until the contour crosses the circle. A point is then interpolated onto the circle using the two points on the movable contour on either side of the circle. The integrals around the arc of the circle are then performed to complete the path, with the flag determining which arcs of the circle belong to the contour integral.

There is an additional limit in the numerical accuracy of the model introduced by the matching conditions. Consider two points on the contour that straddle an intersection of the contour and the edge of the topography (the circle with radius 1). The point just inside the topography has velocity U while the point just outside the velocity has velocity $U(1-h_0)$ due to the conservation of radial transport. Thus, over the next time step, the point over the topography is moved a distance $U\Delta t$ while the point not over the topography is moved $U\Delta t(1-h_0)$. The point originally over the topography can overtake the point not over the topography. This error can create kinks in the contour. The errors associated with this are of the size of the time step Δt, while the error in the time-stepping scheme is order Δt^2, so the results are less accurate because of this. In order to improve the numerical stability of the method, one must reduce the time step. This was done for a case which was initially numerically unstable so that the vorticity was not conserved. When the time step was reduced, the solution became numerically stable and the total amount of vorticity was conserved.

We let h_0/e be the same as in the quasi-geostrophic runs, but change the value of h_0. When the height of the bump is one quarter of the water depth (with a Rossby number of 0.05, figure 11*a*), the system initially evolves more rapidly as the flow is enhanced

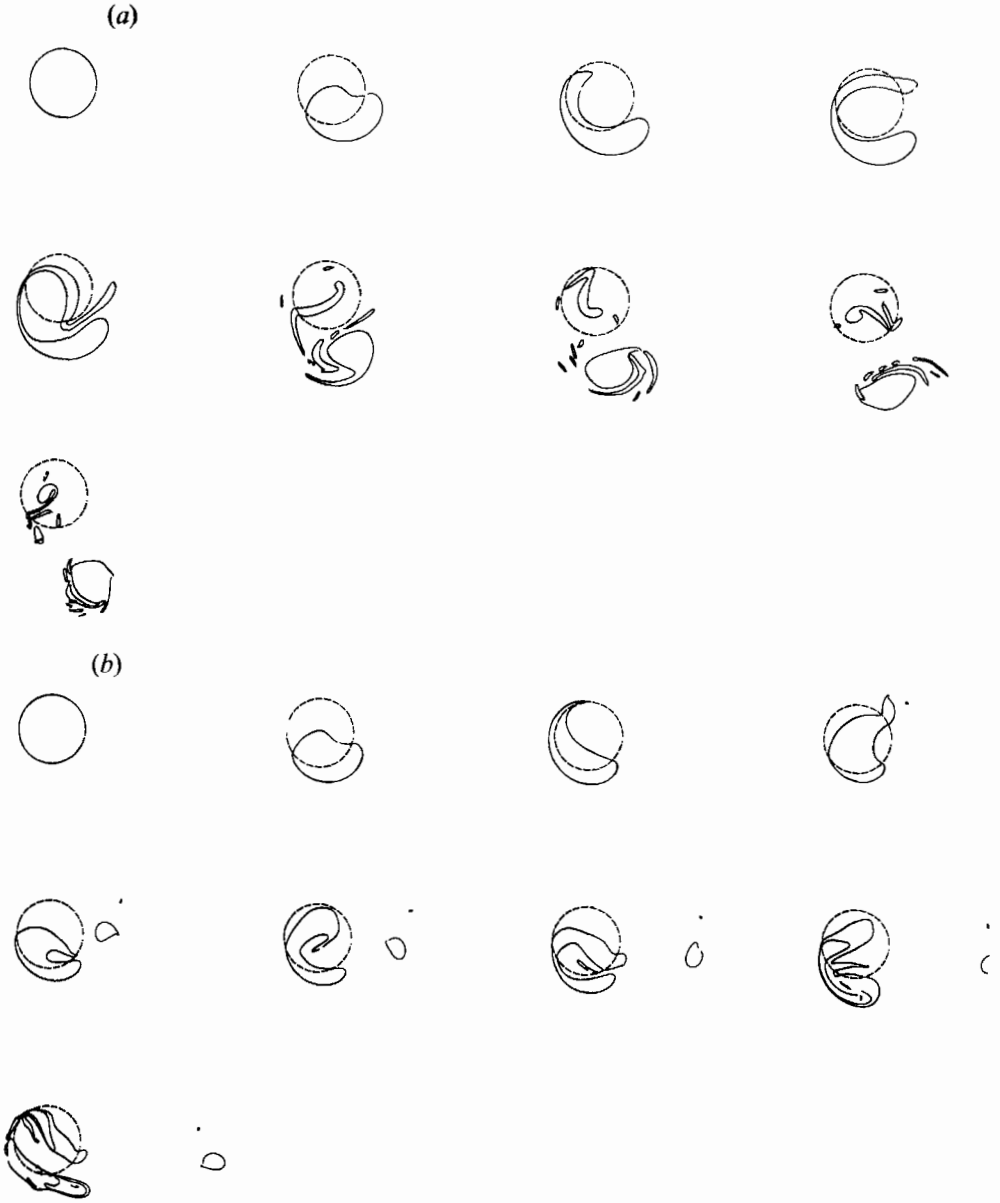

FIGURE 11. Time evolution of the contour for the finite-depth model when $h_0/\epsilon = 5$ for $t = 0, 1, \ldots, 8$. (*a*) $h_0 = 0.25$, and (*b*) $h_0 = 0.5$.

over the topography relative to the quasi-geostrophic solution (figure 7*b*). Later the shed fluid remains closer to the topography and is ejected more to the base of the topography, but eventually escapes downstream as in the quasi-geostrophic case before.

When the topography takes up most of the water column ($h = 0.75$ and Rossby number of 0.15) all of the fluid remains trapped near the topography as it rotates around it in what appears to be a stable oscillation (figure 12). The period of the oscillation is close to two advection times. It is clear here that the area of the contour is not conserved, but the mass is, as the fluid parcels move from shallower to deeper

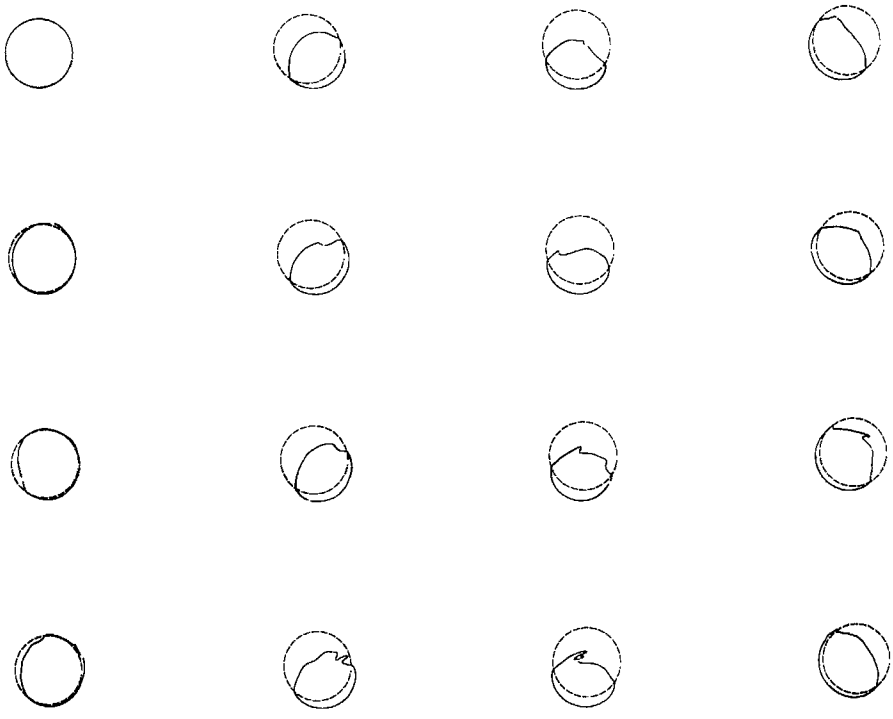

FIGURE 12. Time evolution of the contour for the finite-depth model when $h_0 = 0.75$ and $h_0/\epsilon = 5$ as in figure 7(*b*) for $t = 0, 0.5, 1, 1.5, \ldots, 7.5$.

regions. The oscillation can be understood as a dipole rotating around in a clockwise direction. This is easier to see in the velocity field (figure 13). In fact, if the background flow is turned off after the motion has been initiated (at $t = 2.5$) we find that the oscillation persists, travelling symmetrically around the topography. Oscillations of this sort have been noticed before in time-dependent calculations. Verron & Le Provost (1985) note that in the initial stages of the initial value problem, the fluid seems to be in an oscillatory pattern. James (1980) also noticed this, and in his calculation the oscillation persists for at least four cycles. The oscillation can also be thought of as a nonlinear extension of a seamount trapped wave (Rhines 1969). In the case described here, fluid parcels move on and off the seamount by an order-one amount.

The relationship between the solution of flow over tall topography and flow around an obstacle that reaches to the surface should be mentioned. To solve this problem, the circulation around the island must be specified, and it is normally taken to be zero by the following argument: if the flow starts from rest, and circulation is never introduced into the system, then circulation will never develop. This choice is not the limit of the inertial solution as the topography gets large (i.e. the examples shown in §2), because in that solution vorticity is always produced over the topography. However, the oscillatory solution described above nearly reaches the limit of the island solution as the topography becomes large. This is because none of the fluid escapes downstream, and therefore, vorticity is never produced over the topography. This can be seen in figure 13 in that the flow is nearly symmetric about the x-axis for $r > 1$ throughout the entire oscillation since the net vorticity produced over the topography is very small.

When the Rossby number is increased further ($\epsilon = 0.25$, $h_0 = 0.75$, figure 14), the system seems to approach a steady-state solution, or at least an oscillation with a very

long period. The evolution is similar to that in figure 12, except that the fluid moves completely off the topography while remaining in its vicinity. This value of ϵ coincides with the critical Rossby number above which closed streamlines never occur in the inertial model discussed in §2. This solution is probably related to the steady solutions that Johnson (1978) discussed: indeed, the final pictures look quite similar to his (allowing for the fact that they are not quasi-geostrophic). Furthermore, the evolution has slowed down considerably, suggesting that it is quite closed to a steady equilibrium. Neither solutions of this type, nor the oscillatory solutions, were found in the quasi-geostrophic initial value problem. This appears to be because the acceleration of the flow over the topography in the finite-depth model allows the fluid to be swept off the topography before it has a chance to be deformed by the induced anticyclonic circulation, while there is no acceleration of the background flow in the quasi-geostrophic model.

3.3. *Discussion*

To understand further when different steady or periodic solutions are reached, a regime diagram can be constructed (figure 15), dividing $(h_0/\epsilon,\ \epsilon)$-space into three regions. When $h_0/\epsilon > 1/\epsilon$ the solution is not physically realizable because the topography is larger than the depth of the fluid. In the first region, some of the fluid remains trapped over the topography while some is lost downstream. The appropriate steady-state solution to qualitatively describe these solutions would probably be intermediate retention solutions. In the second region, all of the fluid which originates over the topography escapes downstream. In this case, the inertial solution describes the steady solution near the topography. Finally, in the third region, all of the fluid remains trapped near the topography, either in a periodic oscillation, or in a steady solution similar to the one that Johnson (1978) discussed. None of the quasi-geostrophic solutions ($\epsilon = 0$) fall in this region. The distinction between these two possible solutions is not clear, as it appears that the steady solution arises as a long-period limit of the stable oscillation. The nature of the diagram could certainly change if the background flow were turned on slowly instead of abruptly, since we showed that, at least for the quasi-geostrophic model, the quantitative solution alters. However, one would guess that the three separate regimes would still appear.

4. Conclusions

We have studied flow over finite topography and made comparisons of the solutions to quasi-geostrophic solutions. First, we considered how finite topography affects the flow when the topography has large scale and the β-effect is important. Then, we considered the initial value problem on the f-plane. In both cases, we found that the finite-depth model produced qualitatively different results than those using a quasi-geostrophic formalism. The extensive comparisons were possible because the topography was idealized as a right circular cylinder. In the steady solutions, analytic solutions are possible, and for the time-dependent solution, the efficient method of contour dynamics was used.

The steady solutions can be divided into three parts: the background flow; a component odd in y which is forced by the potential vorticity over the topography; and a component even in y which is forced by the matching conditions on the edge of the topography. In the quasi-geostrophic solutions, the third component does not appear, and, when the topography reaches the surface, the second component is not present. When b is large, we find new effects that are not present in either the f-plane solutions or in the quasi-geostrophic solution. In this limit, the transport is increased over the

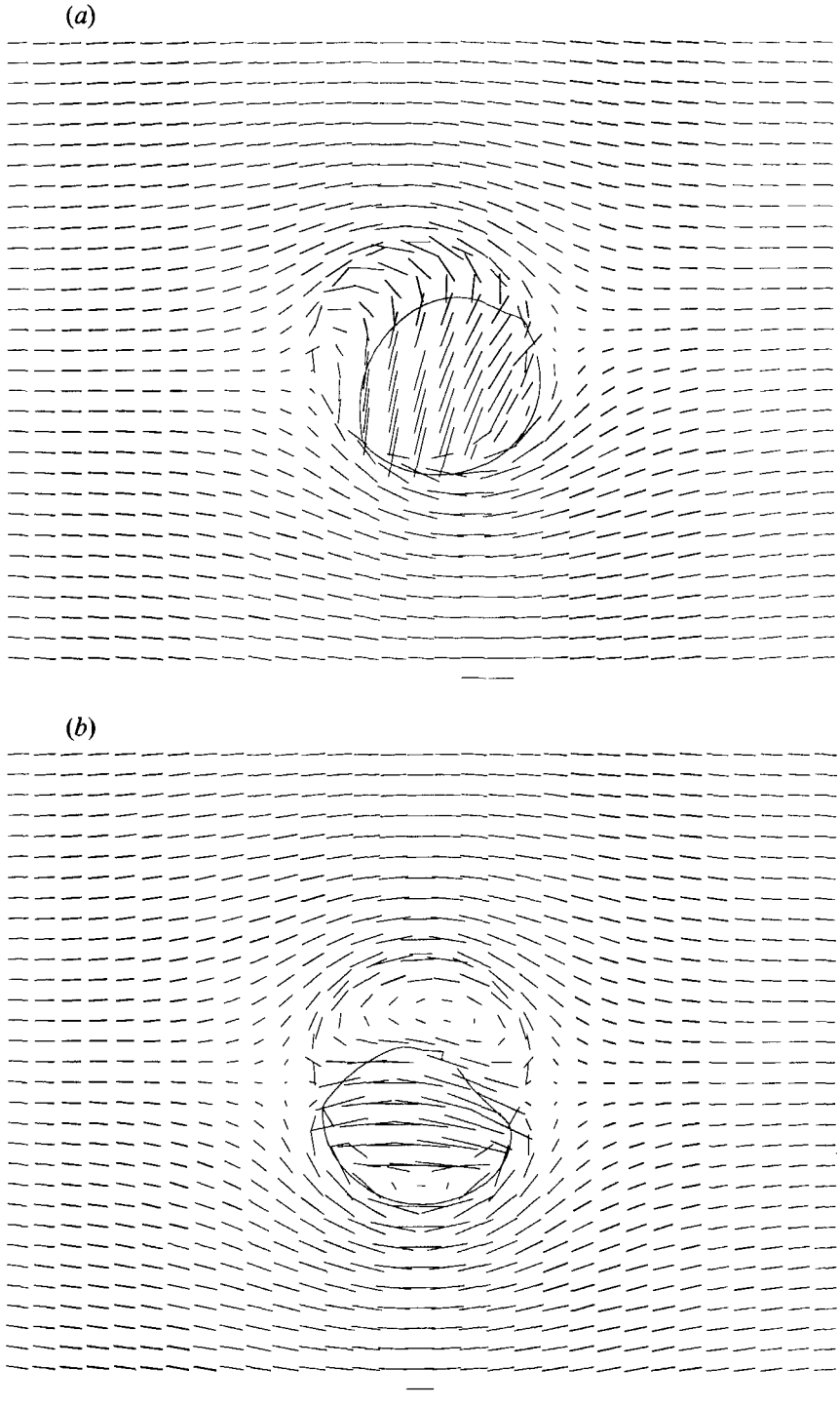

FIGURE 13(*a*,*b*). For caption see facing page.

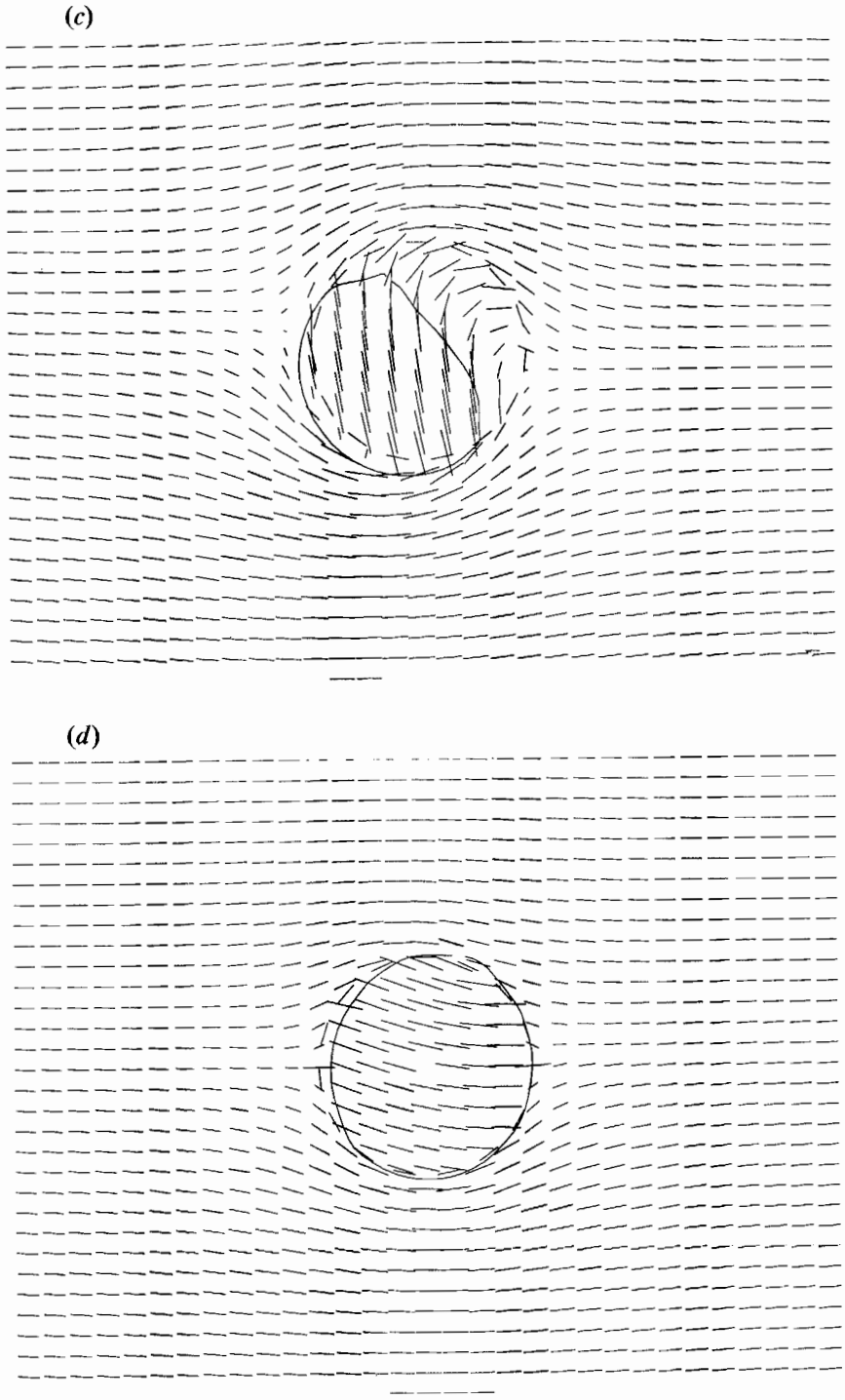

FIGURE 13. Flow field for the case shown in figure 12. (*a*) $t = 0.5$, (*b*) $t = 1$, (*c*) $t = 1.5$, and (*d*) $t = 2$. The background flow goes from left to right. Note that the lines indicate velocity not transport, and the radial velocity is discontinuous at $r = 1$.

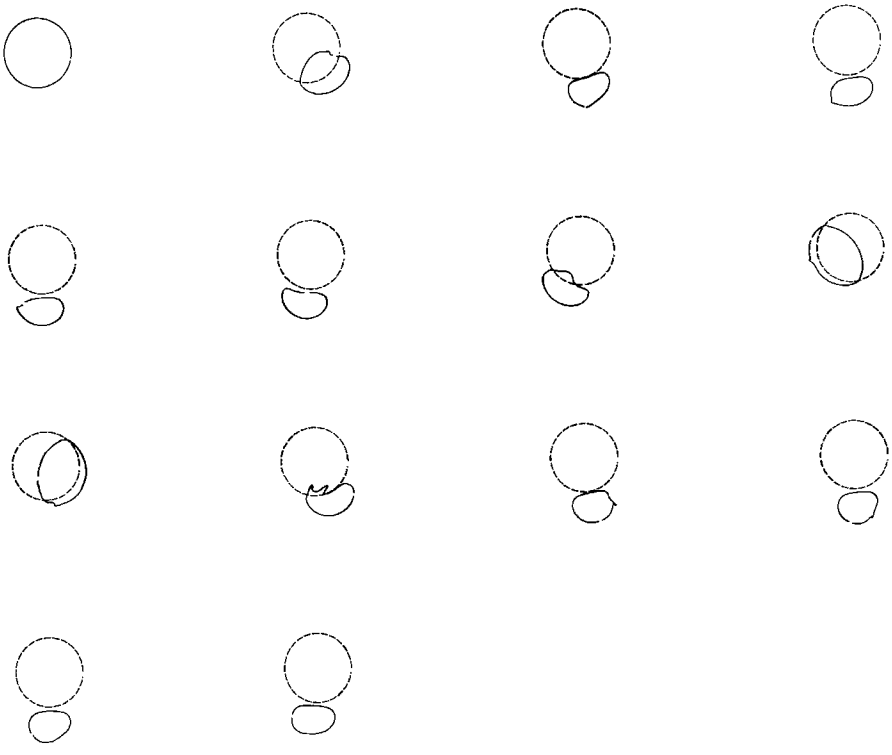

FIGURE 14. Time evolution of the contour for the finite depth model when $h_0 = 0.75$ and $h_0/\epsilon = 3$ as in figure 7(*b*) for $t = 0, 1, \ldots, 13$.

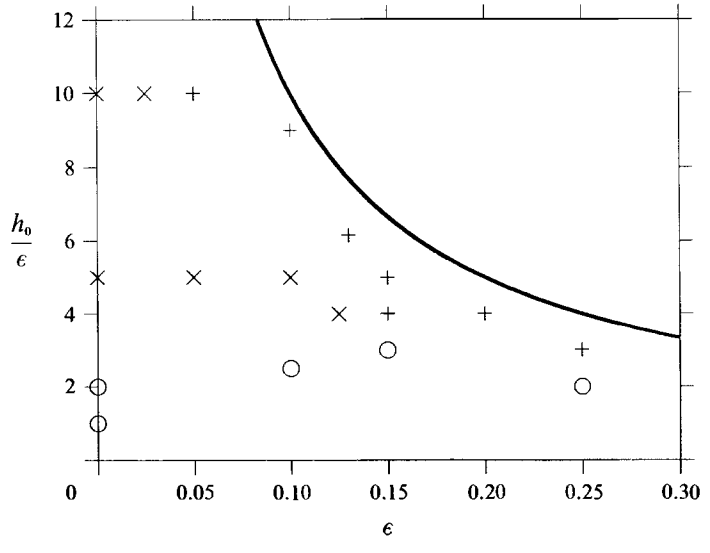

FIGURE 15. Regime diagram for the initial value problem. Above the solid line $h_0 > 1$, which is not allowed; '+' indicates that all of the fluid that originated over the topography is trapped there; '×' indicates that some of the fluid remains trapped, while the rest escapes downstream; and '○' indicates that all of the fluids escapes downstream. The quasi-geostrophic runs appear on the y-axis ($\epsilon = 0$). Above $h_0/\epsilon = 2$ there are closed streamlines in the quasi-geostrophic inertial solution, and for $\epsilon > 0.25$ no closed streamlines exist in the finite-depth inertial solution discussed in §2.2.

topography relative to the background flow for both eastward and westward flow in this regime, a reflection of the tendency for streamlines to follow lines of constant background potential vorticity when the β-effect is large. For eastward flow, the drag can be an order of magnitude larger than that predicted in quasi-geostrophic theory due to the quadratic dependence of the pressure on the velocity found through the conservation of the Bernoulli function.

We examine the initial value problem in the f-plane. We again find new solutions that do not appear in quasi-geostrophic simulations. First we examine flow over quasi-geostrophic topography and show that the time-dependence of the background flow is an important factor in determining how much of the fluid that originated over the topography remains in the initial value problem. We suggest that Johnson's (1983) maximum retention solution can be realized when the flow is turned on smoothly over a long period of time. We construct a family of steady solutions in which only part of the fluid that originated over the topography remains there, and we suggest that one of these solutions is obtained as a quasi-steady state in the initial value problem.

We then consider the initial value problem in the finite-depth model. A new method is developed to apply boundary conditions at circular boundaries, extending the range of problems that can be considered with the method of contour dynamics. We solve the problem separately in two regions, over the topography and away from the topography, using traditional contour dynamics, and then construct zero potential vorticity solutions to match the two regions. This method has more general applications than those explored here (Thompson 1990). A new flow configuration is found in which the fluid which originates over the topography rotates around it in a stable periodic oscillation. Thus, even when the steady inertial solution has no closed streamlines, fluid can be trapped near the topography. When the Rossby number is large, the period of oscillation can become large, and the solution seems to approach the steady solution described by Johnson (1978). A regime diagram is constructed, and it is seen that the quasi-geostrophic system does not exhibit the periodic oscillation for this initial value problem.

The combination of the β-effect and time-dependence have been considered by Verron & Le Prost (1985), but it would be fruitful to include finite topography also so that all three effects could be considered simultaneously. More realistic geometry would also be desirable, though, of course, the simplified geometry allows a more thorough exploration of parameter space than would otherwise have been possible.

This research was supported by the Office of Naval Research Program N00014-90-J-1839 and was done while L.T. was a student in the MIT-WHOI Joint Program in Oceanography. Additional work was done by L.T. under the College of Oceanography and Fisheries Sciences fellowship at the University of Washington. We thank Steve Meacham for sharing his contour dynamics programs with us.

Appendix

We expect that the shallow-water model will be valid as long as the aspect ratio of the fluid is small. Therefore, when the topography is steep, its validity is questionable. To examine the range of validity, we consider rotating barotropic flow onto a shelf with depth $h(x)$. The flow is assumed to be independent of y except for a uniform northward pressure gradient. Under the shallow water approximation, the momentum equations are

$$uu_x - fv = -P_x,$$

and $$uv_x + fu = -P_y,$$

and the continuity equation is

$$(hu)_x = 0.$$

Upstream of the shelf, $fu_0 = -P_y$. The potential vorticity equation is then

$$(v_x + f)/h = f/h_0,$$

where h_0 is the depth of the fluid far upstream of the shelf. Then

$$u = h_0 u_0/h,$$

and

$$v = \frac{f}{h_0}\int_{-\infty}^{x} (h - h_0)\,\mathrm{d}x.$$

Thus, under the shallow-water approximation, the meridional velocity v is continuous across the shelf, no matter how steep the topography is. Note that the flow is not geostrophically balanced to the east, which can be seen by applying the solution given above to the meridional momentum balance.

To see when the shallow-water solution breaks down we consider the same problem using the full momentum equations. We can define a stream function such that $u = -\psi_z$ and $w = \psi_x$ so that the momentum equations become

$$J(\psi, u) - fv = -p_x, \quad J(\psi, v + fx) = fu_0, \quad J(\psi, \omega) = -p_z, \tag{A 1}$$

where the Jacobean is

$$\psi_x \partial/\partial z - \psi_z \partial/\partial x.$$

Once again the solution is independent of y except for the uniform northward pressure gradient. A horizontal vorticity equation can be formed

$$J(\psi, \nabla^2\psi) + fv_z = 0. \tag{A 2}$$

The problem in (A 1) and (A 2) can be solved subject to the boundary conditions

$$\psi = 0, \quad z = 0,$$
$$\psi = u_0 h_0, \quad z = -h,$$
$$h \to h_0, \quad x \to -\infty,$$
$$\psi \to -u_0 z, \quad x \to -\infty.$$

The problem (A 1)–(A 2) is nonlinear and not easily solved, but we can examine the form which leads to the shallow-water solution in order to determine what the errors are. Under the shallow-water approximation,

$$\psi = -u_0(h_0/h)z.$$

Putting this solution into the northward momentum equation (A 1) gives

$$u_0 h_0 \frac{v_x + f}{h} + \frac{u_0 h_0 z h_x v_z}{h^2} \approx fu_0. \tag{A 3}$$

Note that the first term here, balanced with the right-hand side, gives the shallow-water potential vorticity expression. The second term should be small if v_z is small. It can be estimated using the vorticity equation (A 2)

$$fv_z \approx -u_0^2 h_0^2 z\left[\left(\frac{\partial}{\partial x}\frac{1}{h}\right)\left(\frac{\partial^2}{\partial x^2}\frac{1}{h}\right) - \frac{1}{h}\frac{\partial^3}{\partial x^3}\frac{1}{h}\right].$$

If the lengthscale of the topography is L the scale estimate of the vertical shear is then

$$v_z \approx u_0^2 h_0 / f L^3,$$

and the ratio of the second term in (A 3) to the first (on the right-hand side) is

$$(u_0/fL)^2 (h_0/L)^2,$$

suggesting the limits of validity of the shallow-water model.

Given small aspect ratio, so that the shallow-water model is valid, the change in v across the topography is

$$v(L) - v(0) = f \int_0^L \frac{h - h_0}{h_0} \approx fL$$

so that for the shallow-water solution to be valid, L must be small compared to the radius of the bump, but large compared to

$$(u_0 h_0 / f)^{\frac{1}{2}}.$$

When these requirements hold, the shallow-water approximation can be applied and the correct matching conditions on the boundary of the topography are those used in this paper.

REFERENCES

BANNON, P. R. 1980 Rotating barotropic flow over finite isolated topography. *J. Fluid Mech.* **101**, 281–306.

BOYER, D. L., DAVIES, P. A. & HOLLAND, W. R. 1984 Rotating flow past disks and cylindrical depressions. *J. Fluid Mech.* **141**, 67–95.

HIDE, R. 1961 Origin of Jupiter's Great Red Spot. *Nature* **190**, 895–896.

HUPPERT, H. E. 1975 Some remarks on the initiation of inertial Taylor Columns. *J. Fluid Mech.* **67**, 397–412.

HUPPERT, H. E. & BRYAN, K. 1976 Topographically generated eddies. *Deep-Sea Res.* **23**, 655–697.

INGERSOLL, A. P. 1969 Inertial Taylor Columns and Jupiter's Great Red Spot. *J. Atmos. Sci.* **26**, 744–752.

JAMES, I. N. 1980 The forces due to geostrophic flows over shallow topography. *Geophys. Astrophys. Fluid Dyn.* **9**, 159–177.

JANOWITZ, G. S. 1975 The effect of bottom topography on a stratified flow in the beta plane. *J. Geophys. Res.* **80**, 4163–4168.

JOHNSON, E. R. 1977 Stratified Taylor columns on a beta-plane. *Geophys. Astrophys. Fluid Dyn.* **9**, 159–177.

JOHNSON, E. R. 1978 Trapped vortices in rotating flow. *J. Fluid Mech.* **86**, 209–224.

JOHNSON, E. R. 1979 Finite depth stratified flow over topography on a beta-plane. *Geophys. Astrophys. Fluid Dyn.* **12**, 35–43.

JOHNSON, E. R. 1983 Taylor columns in a horizontally sheared flow. *Geophys. Astrophys. Fluid Dyn.* **24**, 143–164.

JOHNSON, E. R. 1984 Starting flow for an obstacle moving transversely in a rapidly rotating fluid. *J. Fluid Mech.* **149**, 71–88.

KOZLOV, V. F. 1983 The method of contour dynamics in model problems of the ocean topographysical cyclogenesis. *Izv. Atmos. Ocean Phys.* 635–640.

MEACHAM, S. P. 1991 Meander evolution on quasi-geostrophic jets. *J. Phys. Oceanogr.* **21**, 1139–1170.

MCCARTNEY, M. S. 1975 Inertial Taylor columns on a beta plane. *J. Fluid Mech.* **68**, 71–95.

MCKEE, J. W. 1971 Comments on 'A Rossby wake due to an island on an eastward current.' *J. Phys. Oceanogr.* **1**, 287.

MILES, J. W. & HUPPERT, H. E. 1968 Lee waves in a stratified flow. Part 2. Semi-circular obstacle. *J. Fluid Mech.* **33**, 803–814.

POLVANI, L. M. Geostrophic vortex dynamics. Ph.D thesis, MIT/WHOI, WHOI-88-48.

RHINES, P. B. 1969 Slow oscillations in an ocean of varying depth. Part 2. Islands and seamounts. *J. Fluid Mech.* **37**, 191–205.

TAYLOR, G. I. 1917 Motion of solids in fluids when the flow is not irrotational. *Proc. R. Soc. Lond.* A **93**, 99–113.

TAYLOR, G. I. 1923 Experiments on the motion of solid bodies in rotating fluids. *Proc. R. Soc. Lond.* A **104**, 213–218.

THOMPSON, L. 1990 Flow over finite isolated topography. PhD thesis, MIT-WHOI, WHOI-91-05.

VERRON, J. & LE PROVOST, C. 1985 A numerical study of quasi-geostrophic flow over isolated topography. *J. Fluid Mech.* **154**, 231–252.